

A COMPARATIVE STUDY ON THE PERFORMANCES OF DIFFERENT PROPELLER DESIGNS



MAY 26, 2016
SUPERVISOR: PROF.KARINA HJELMERVIK
STUDENT: YANNI CHANG

Abstract

The designed propellers with extinguishing structures of hub and winglets show great potential in saving energy by providing the strong thrust with a rotating speed. The dynamic performances are relying on the combination of geometries characteristics. This project is based on a cooperation with Nodin Innovation since August 2015 to study different propeller hubs and winglets through FEM modelling.

Hub structures in convex, concave, dome, and dome coping with a small Center propeller located on the front of the hub are tested with a rotating speed under the RPM of 100 rev/min in manipulation under the standard $k-\varepsilon$ turbulence model. The shear stress transport turbulence model is carried out to study the potential dynamic properties of four propellers (the Convex propeller, the Dome propeller, the Center propeller, and the Winglet propeller) under the RPM less than 3000 rev/min. The mass flow through the inlet, interfaces, and the outlet is applied to determine the stability of the fluid flow. The present study shows a relative mass flow of each propeller compared with the Convex propeller which is chosen to be the reference model in this dissertation.

Through CFD simulations in ANSYS CFX, we evaluate the dynamic performances of the designed propellers. Some tables and figures containing the most important parameters, and the expecting future work are given to open up a specific avenue for improving the analysis process for the simulations.

Acknowledgements

I gratefully commend the support and the help from Assoc.Prof. Karina Hjelmervik from the University College of Southeast Norway in this master project. I would like to express my thankfulness sincerely to my supervisor Assoc.Prof. Karina Hjelmervik, for her great patience and guidance that she has given to me to accomplish the thesis for her scientific contribution and supervision. I am also deeply impressed by her kindness to show me around the natural and beautiful Norwegian life, and the Viking culture during my master time. All the tips about living in Norway from her make my life in Norway enjoyable and unforgettable.

The work summarized here is also part of Nodin Innovation project about propellers, in which I used the 3D models designed by Mr. Finn Limseth and Mr. Rune Østigård. With thankfulness towards the two gentlemen, I will express my gratitude to them for the help designing and establishing models in ANSYS. Thanks again to Mr. Finn Limseth invited Assoc.Prof. Karina and I to visit the company for checking real models, the industry equipment, and the systems of the commercial ships, which leads a great inspiration for me as well as lightens the meaning of my work connected with people's daily life.

Thanks again to Mr. Rune Østigård who shared his vision and the many years' working experience of being an engineer with me, his encouragement and good wishes for my future will be always memorized on my way to be a qualified engineer.

I also want to thank all my friends. I learnt different kinds of culture, learnt several ways to make a greeting, and tasted wonderful food with them. The two-year time in Norway is not only a program training my skills but also a rainbow colored my life.

Finally I would like to express my thankfulness to my father and my mother. They are always my support no matter what has happened and will happen.

Symbols

Latin letters

D	Diameter-Overall diameter of the propeller
N	Rotation rate-Rotation speed of the propeller in rev/min
T	Thrust-Propeller axial thrust force
Q	Torque-Propeller shaft torque
V_s	Ship speed-Ship velocity
V_a	Inflow velocity-Mean inflow velocity
V_A	Speed of the propeller relative to the disturbed surrounding water
P_s	Shaft power
P_E	Effective power

Greek letters

ρ	Fluid density
--------	---------------

Abbreviation

CFD	Computational Fluid Dynamics
RPM	revolution/minute
NS Equations	Navier-Stokes equations
GGI	General Grid Interface
LES	Large Eddy Simulation
RANS	Reynolds-averaged Navier-Stokes
V&V	Verification and Validation
DNS	Direct Numerical Simulation
RNG	Renormalization Group
P.C.	Propulsive Coefficient
RSM	Reynolds Stress Model
SST	Shear Stress Transport
CFL	The Courant-Friedrichs-Lewy Criterion

Table of contents

Abstract	i
Acknowledgements	ii
Symbols	iii
Abbreviation	iv
Table of contents	v
Tables of figures	vii
List of table	ix
<i>Chapter1 Introduction</i>	<i>1</i>
1.1 Background and History	2
1.2 Fundamentals in Propeller Design.....	2
1.3 Motivation and Goal.....	6
1.4 Structure of the Thesis.....	6
<i>Chapter 2 Mathematical Formulation and Implementation</i>	<i>8</i>
2.1 Propeller Propulsion	8
2.2 Mass Flow	8
2.3 Continuity Equations	9
2.4 Navier-Stokes Equations	10
2.5 Turbulence Model.....	10
<i>Chapter 3 Methodology and FEM Analysis</i>	<i>14</i>
3.1 Geometry Description.....	14
3.2 Mesh	18
3.3 Set-up of Mesh.....	19
3.4 Set-up in Analysis Part	32
3.5 Analysis Type	36
<i>Chapter 4 Results from Numerical Simulations</i>	<i>38</i>

4.1	The Courant-Friedrichs-Lewy (CFL) criterion.....	38
4.2	Reference Number for Mass Flow of Convex propeller.....	40
4.3	Different Propeller Models and RPMs	45
<i>Chapter 5</i>	<i>Discussion</i>	52
5.1	Compared Results of Propellers	52
5.2	Discussion of Growing Velocity	55
5.3	Recommendation for Future Work.....	58
<i>Chapter 6</i>	<i>Conclusion</i>	60
Bibliography	61

Tables of figures

Figure 1-1 The fixed-pitch propeller from Kamome Propeller Company in Japan	3
Figure 1-2 Propeller definition diagram	4
Figure 1-3 Cross section of propeller blade	5
Figure 3-1 Geometry of Convex propeller	15
Figure 3-2 Geometries of propellers	15
Figure 3-3 Boeing 737-700 with blended winglets	17
Figure 3-4 The basic elements of three dimensional cell shapes	19
Figure 3-5 Positions and names of the Convex propeller	21
Figure 3-6 Mesh of the Convex propeller	23
Figure 3-7 Cross section of the mesh of Convex propeller	25
Figure 3-8 Zoomed in mesh of the blades, tips, and the tunnel of Convex propeller	25
Figure 3-9 Mesh of the transition of Convex propeller between Domain A and Domain B ...	26
Figure 3-10 Cross section in XY plane of Concave propeller with inflation rate of 1.05	28
Figure 3-11 Cross section in XY plane of Dome propeller with inflation rate of 1.05	28
Figure 3-12 Cross section in XY plane of Center propeller with inflation rate of 1.05	29
Figure 3-13 Cross section in YZ plane of Torqeedo propeller with inflation rate of 1.06	30
Figure 3-14 Cross section in XZ plane of Winglet propeller with inflation rate of 1.06	31
Figure 3-15 Ramp function	34
Figure 4-1 Monitored velocity in X direction of Convex propeller at RPM of 100rev/min with total time of 10s, and the time step of 0.005s	39
Figure 4-2 Time-step and CPU time with different total time	40
Figure 4-3 Difference of mass flow between interface BC and outlet	41
Figure 4-4 Different mass flow changed by time step within 2s, 1s, and 0.5s	42

Figure 4-5 Mass flow at the outlet with RPM of 3000rev/min	43
Figure 4-6 CPU time and time step with RPM of 3000rev/min.....	43
Figure 4-7 CPU time and time step with RPM of 1500rev/min.....	44
Figure 4-8 Mass flow at the outlet with RPM of 1500rev/min	45
Figure 4-9 Mass flow at outlet as a function of RPM for four propellers.....	46
Figure 4-10 Relative mass flow as a function of RPM for different geometries	47
Figure 4-11 Mass flow at outlet and RPM of propellers.....	48
Figure 4-12 Monitor results of the whole simulation with the Dome propeller at RPM of 1500 rev/min within total time of 1s and the time step of 0.03s	49
Figure 4-13 Monitor results of the whole simulation with the Dome propeller at RPM of 1250 rev/min within total time of 1s and the time step of 0.05s	50
Figure 5-1 Hub part of the Concave propeller (left), the Convex propeller (middle), and the Dome propeller (right)	52
Figure 5-2 Geometry of equilibrium raindrop shapes.....	53
Figure 5-3 Velocity vectors of Convex propeller with total time of 10s and the time step of 0.005s	55
Figure 5-4 Velocity vectors of Convex propeller with total time of 2s and the time step of 0.005s	56
Figure 5-5 Velocity vectors of Convex propeller with total time of 1s and the time step of 0.005s	57

List of table

Table 3-1 Mesh option and the positions	20
Table 3-2 Definitions of the face sizing of Convex propeller model.....	21
Table 3-3 Inflation options for the Convex propeller model	22
Table 3-4 Definitions of contacting size	23
Table 3-5 Mesh statistics for Convex propeller	24
Table 3-6 Statistic of mesh metric of Convex propeller	27
Table 3-7 Mesh statistics of the Concave propeller	27
Table 3-8 Size statistic of the elements of Convex propeller.....	27
Table 3-9 Mesh statistics of Dome propeller	29
Table 3-10 Mesh statistics of Center propeller	30
Table 3-11 Mesh statistics of Toqeedo propeller	30
Table 3-12 Mesh statistics of Winglet propeller	31
Table 3-13 Setting options of Domain A	32
Table 3-14 Setting options of Domain C	33
Table 3-15 Setting options of Domain B	35
Table 3-16 Global settings regarding initialization.....	35
Table 4-1 Mass flow at Outlet with RPM of 1500 rev/min	49
Table 4-2 Mass flow and RPM for Winglet propeller	51
Table 5-1 Mass flow at RPM of 1500 rev/min with the time step of 0.03s	54

Chapter1 Introduction

During the recent decades, computer simulations of the physical processes have been applied into the scientific research and in the analysis and design of engineered systems. The systems of interest are existing or proposed systems that can work at design conditions, off-design conditions, failure-mode conditions, or accident scenarios [1]. Though the roots of Computational Fluid Dynamics (CFD) can be traced back to the 1920s, CFD has made a rapid progress in the industry since 1960s. In this context, the investigation into predicting the dynamic properties within the commercial ships propellers using CFD modelling methodology is of extreme importance and can help assist structural geometries applications [2]. With a flourish of techniques of CFD, a new avenue is opening up for the research about optimizing geometries for propellers with highly predicted Reynolds averaged Navier Stokes solutions. Despite such progress has been achieved in both code and facility developments, these CFD simulation-based predictions are five to eight year earlier than what was eventually realized, even for specialist CFD practitioners and aerodynamicist in the design office [3]. The CFD technology has provided a perception in computing complex conditions with specific factors and assumptions, where the traditional experiments show limitations in producing more realistic results.

With the assistance from the CFD technology, the time and human cost can be greatly reduced to figure out which geometry performs better among all the designed models from Nodin Innovation. Besides the appropriate solutions from the well-established models like standard $k-\varepsilon$ turbulence model and the shear stress transport turbulence model, the CPU time dependent on the time-step according to the Courant-Friedrichs-Lewy criterion (CFL), there are some other significant issues to be considered (for example, the cost of the time spent on setting up CAD geometries and mesh grids). The thesis will pay attention to find the fine meshes for the models and reduce the CPU time simultaneously by choosing a proper time step.

In the master thesis, studies and analyses of numerical models for the new designed propellers from Nodin Innovation respectively, are presented. The comprehensive analyses of the effect of various parameters (for example, mesh characteristics, total time, and the time step of the analyses in setting up modules) on the simulated results are reported, together with a comparison with the same settings but different geometries.

The feasibility of the CFD technology has a significant impact reducing in time and cost compared with undertaking an experiment [4]. Despite all the benefits provided from CFD technology, there still are some future work for this thesis.

1.1 Background and History

Computational Fluid Dynamics (CFD) has now matured to the status at which it is commonly used as a computer aided tool the propeller design due to the flourish development of the large high-speed computers. Navier-Stokes equations establish the fundamental basis for most CFD problems by defining the fluid flows. Euler equations are approached with the simplifications of the Navier-Stokes equations via removing the items of the viscosity [5].

Lewis Fry Richardson proposed a calculation method resembling modern CFD but failed pitifully. In Richardson's book "Weather prediction by numerical process" [6], the calculations and the numerical meteorology [5] were described in 1965. At the same time period, the Los Alamos Scientific Laboratory (now the Los Alamos National Laboratory) started focusing on the subject of numerical models in the field of fluid mechanics from 1957 to late 1960s [7]. They opened up a new avenue to simulate the transient two-dimensional fluid flow, such as Particle-in-cell method(Harlow,1957) [8], with the implementation of MANIAC computer aided with their division work. It can be recorded that the first paper about 3-D model which was applied by the panel methods was published by John Hess and A.M.O. Smith of Douglas Aircraft in 1967 [5]. After many CFD studies, people started manipulating the Navier-Stokes equations to solving commercial engineering problems.

It is recorded that the paddle-wheel-propelled ships were used to transport people by pre-Christian, leading an inspiration to apply mechanical forces of the water to establish propulsion systems for the vessels. Leonard da Vinci was famous for designing some pieces of propulsive equipment. There was a well-known comparison between the stream vessels named Rattler, which was screw propelled, and its small scaled similar ship, the Alecto, which was paddle powered in 1845 [9].

1.2 Fundamentals in Propeller Design

The geometry configuration of a propeller is widely acknowledged to be one of the most important features taken account of the complexities and physical properties of the propellers. With many years' development, some efficient designs of propellers have already been applied

to the commercial ships. Here lists some propellers with good performances within categories [9].

- Screw propellers
 - Fixed-pitch propellers
 - Adjustable-pitch propellers
 - Controllable-pitch propellers
 - Ducted propellers
 - Contra-rotating propellers
- Paddle wheels, either side or stern mounted with fixed or feathering blades
- Jet propellers
 - Water jet through submerged nozzle
 - Water jet through surface nozzle
- Vertical-axis propellers
 - Kirsten-Boeing propeller
 - Voith-Schneider propeller



Figure 1-1 The fixed-pitch propeller from Kamome Propeller Company in Japan
which is the core product in this company [32]

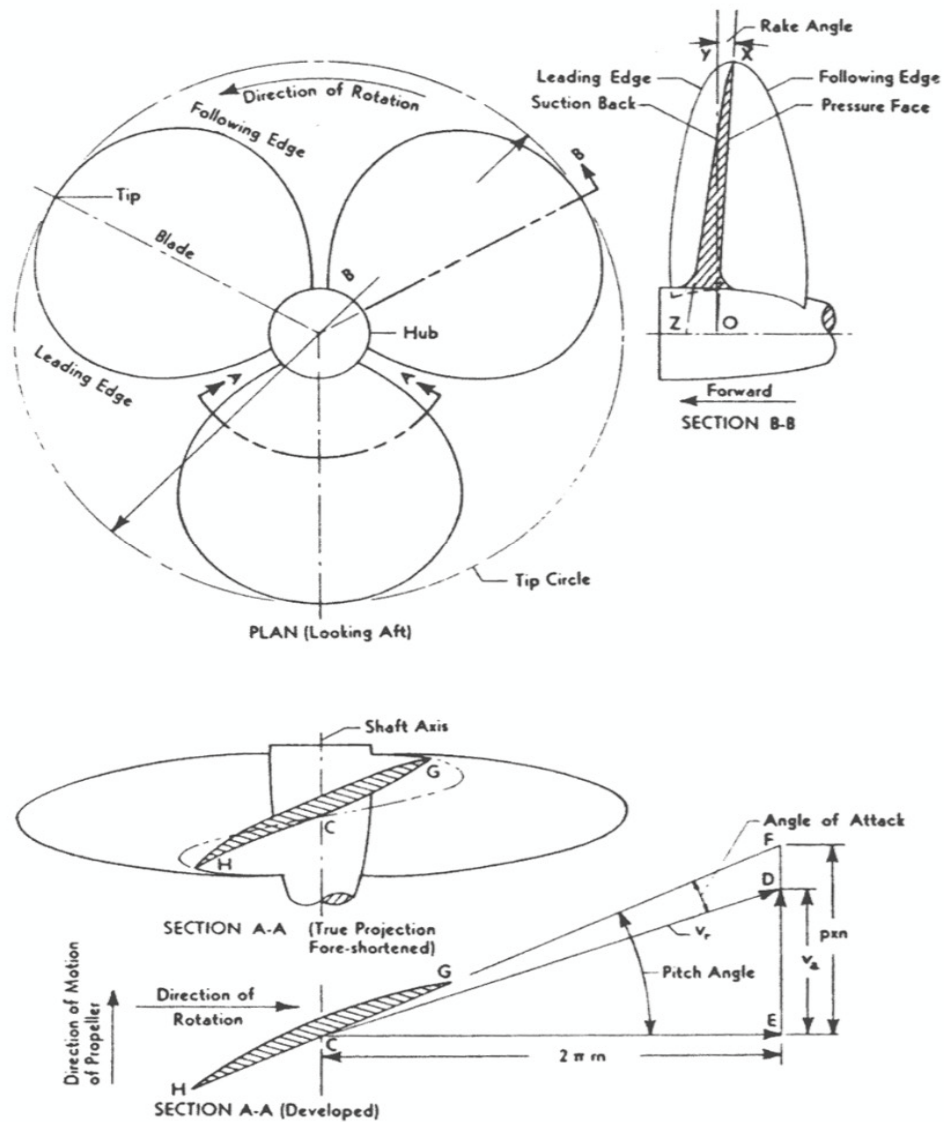


Figure 1-2 Propeller definition diagram

(three-bladed, right-handed, constant-pitch propeller) [9]

The screw propeller is one of the most commonly used propellers in terms of its sound and strong connection with the propulsive theories of fluid mechanics. The screw propeller usually consists of at least two blades to provide force in the propulsive system.

There are three general types of marine propellers are widely used in the world now.

- Fixed-pitch propellers

There are two different types of blades applied in this kind of propellers in terms of the positions for the blades relative to the hub. One type has an integral part of the hub, the

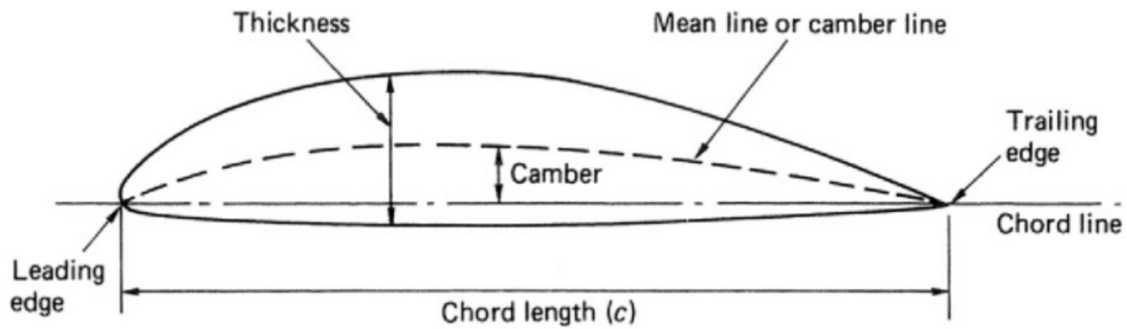


Figure 1-3 Cross section of propeller blade
with defined names on the cross section [9]

other designs a bolt part to connect with the hub [9]. The structure of the fixed-pitch propellers is shown in Figure 1-1 .

- Adjustable-pitch propellers

The relative position between the blades and the hub can be operated by these kinds of propellers at any time. In the Figure 1-2, it shows the configuration of a three-blade propeller of constant-pitch [9].

A right-handed propeller rotates in the direction of clockwise when it is looked astern.

The cross section of the propeller blade is similar to the airfoil. The definitions of the geometry of the propeller are coping with the Figure 1-3 [10] .

- Mean line (Camber line): the length of the middle point between the upper and lower surface of the blade with a perpendicular measurement to the camber line.
- Nose-Tail line: straight distance between the mean line point of the leading edge and mean line point of the trailing edge.
- Chord length: the distance of the Nose-Tail line.
- Camber height: the length of the measurement between Nose-Tail line and the mean line perpendicular to the Nose-Tail line.
- Thickness: it is the section thickness perpendicular to the mean line, as a function of chord wise position

1.3 Motivation and Goal

The CFD simulations are applied into the investigation for different geometries of the propellers, trying to analyze the performances within the open water environment.

A series of simulations results from different designed models will be presented, in order to provide an insight into the dynamic behavior from various geometries of the hubs, and the winglets. The design of traditional propeller is conventionally based on the Betz criteria (Lerbs, 1952), following the requirements of the flow downstream of the propellers, taken account of the minimum energy loss [11]. It is possible to conclude that the velocity and relative mass flow among changed designs with implementation in ANSYS CFX mode is in good agreement to provide suggestions for the structures of the propellers.

Leisure boats require a much higher velocity than the commercial ships as it is generally acknowledged that the heavier boat requires the lower propeller pitch [12]. This master thesis is in cooperation with a Norwegian company named Nodin Innovation. The conventional propellers sometimes neglect the optimal design structure of the hubs, as well as the winglet part. The influences of these configurations within one propeller will be taken account of the performances, which are expecting to overcome some limitations from the traditional propellers, allowing for a better efficient structure design for optimization.

1.4 Structure of the Thesis

With a brief introduction of the history, the background of the CFD, and its application, two main turbulence models are implemented into simulations with different rotating speeds. The standard $k - \varepsilon$ turbulence model is applied into the low speed (RPM less than 100 rev/min) simulations with Convex propeller, Concave propeller, Dome propeller, and Center propeller while the shear stress transport turbulence model is manipulated to investigate the performances with the Convex propeller, the Dome propeller, the Center propeller, and the Winglet propeller, which all work with the high rotating speed (RPM less than 3000 rev/min, and higher than 500 rev/min). First of all, geometries of propellers are described with details. A sound mesh is highly desirable to develop reliable grids with the limitation of the nodes and elements, the computational time, and the captured physics. Secondly, the total time and a proper time step have drawn great attention due to the CFL criteria and the computational time of the computer. The rest of the thesis is organized as follows.

In 3.4, after checking the stability of the flow, relative mass flow is calculated, which approaches the summary of the propellers' performances. However, there are some refinements left to be done in the future. We denote two different mesh settings for the propellers in low and high rotating speed, but the time step is not small enough to provide a stable fluid flow. With the restriction of the computational time, the time step used in this study is considered to be applied into propeller models but with some errors. At last, the future work is proposed for improving the accuracy.

Chapter 2 Mathematical Formulation and Implementation

2.1 Propeller Propulsion

The thrust is referred to as the force operated by the rotating propellers. In order to overcome the resistance of the ship, the thrust increases until reaching a balance between the resistance and the thrust considering the fact that the resistance is also increasing with the speed of the vessel. However, in this study, the models we established to describe the propellers are without the resistance forces, which means the velocity of the fluid flow will increase with time and will never achieve a balance condition. The thrust can be expressed in the following equation [9].

$$T = \rho A v_1 (v_b - v_a) \quad (2-1)$$

Where T = thrust

ρ = water density (mass)

A = area of the projected propeller disc

v_1 = velocity through the propeller

v_a = velocity ahead of the propeller at X

v_b = velocity behind of the propeller

In our models, the v_a and v_b has little difference because of the lack of the resistances from the vessel. Therefore, we cannot use the thrust to calculate the dynamic performances. Compared to the conventional approaches, the mass flow is applied to the simulations for comparing the propellers. As a proof-of-concept, a bigger thrust will drag more water to pass through the propeller which refers to a larger mass flow through the propeller.

2.2 Mass Flow

It is generally acknowledged that the mass flow passing through the specific surface per second is the mass flow rate, named mass flow in this study.

$$\dot{m} = \rho AV \quad (2-2)$$

Where:

ρ is the density of the fluid, it refers to the water in this study, with the fluid temperature of $25^\circ C$.

A is the area of the surface which the fluid goes through.

V is the mean velocity of the flow which can be monitored by ANSYS CFX.

The mass flows generated by different propellers will be compared to check the performances of the propellers.

2.3 Continuity Equations

According to the conservation principles of mas, momentum and energy, the continuity equation is given by formula (2-3).

$$\frac{d}{dt} \int_{\Omega} \phi dV = - \int_{\partial\Omega} \phi u \cdot ndA - \int_{\Omega} s dV \quad (2-3)$$

Where ϕ is the intensive property, Ω is the control volume, u is the velocity of the fluid flow, and s is the sources and sinks in the flow.

After combining the divergence theorem and Leibniz's rule, the integral must be zero for any control volume, therefore a new equation is given by:

$$\frac{\partial \phi}{\partial t} + \nabla \cdot (\phi u) + s = 0 \quad (2-4)$$

There are two important equations applied with the mass and the momentum [13].

Conservation of mass:

$$\frac{\partial \rho}{\partial t} + \nabla \cdot (\rho u) = 0 \quad (2-5)$$

Where ρ is the density of the fluid.

When the flow is considered as an incompressible flow, ρ will not be a function of time and space.

The simplification of the equation of the conservation of mass is given by formula (2-6).

$$\nabla \cdot v = 0 \quad (2-6)$$

Conservation of momentum:

$$\frac{\partial}{\partial t}(\rho v) + \nabla(\rho v \otimes v) = \sum \rho f \quad (2-7)$$

Where the $v \otimes v$ is a tensor, \otimes means the tensor product.

2.4 Navier-Stokes Equations

The Navier-Stokes equations are proposed independently by Navier in 1823 and Stokes in 1845. The Navier-Stokes equations are based on the assumption that the fluid is in a continuum. In other words, the fluid is continuous without discrete particles. Another assumption of Navier-Stokes Equations is that all the terms like velocity, pressure, density, temperature, and other parameters are all differentiable [14]. Under a definition of control volume, which refers to the finite arbitrary, the Navier-Stokes equations are derived from the fundamental principles of continuity of mass, momentum and energy via Reynolds transport theorem [14].

The general equation is given as:

$$\frac{\partial u}{\partial t} + (u \cdot \nabla)u = f - \frac{1}{\rho} \nabla p + \nu \nabla^2 u \quad (2-8)$$

Where:

$\nu = \mu/\rho$ is the kinetic viscosity.

$\nabla p = i \frac{\partial p}{\partial x} + j \frac{\partial p}{\partial y} + k \frac{\partial p}{\partial z}$ is the pressure gradient.

$\nabla^2 = \frac{\partial^2}{\partial x^2} + \frac{\partial^2}{\partial y^2} + \frac{\partial^2}{\partial z^2}$ is the Laplace operator.

Each item in the equation refers to the unit mass of the flow.

2.5 Turbulence Model

It is impossible to apply a single turbulence model to all fluid problems. The Reynolds Averaging Navier-Stokes (RANS) equations are induced to solve the Direct Navier-Stokes

(DNS) equations about turbulent flows. Specific models are required to capture characteristics of specific turbulent models via coping with the motion of the fluid, in order to establish accurate mathematical models to present the realistic movement [15].

The Boussinesq family is the origin of the following listed turbulence models: the standard $k - \varepsilon$ model, RNG $k - \varepsilon$, realizable $k - \varepsilon$, standard $k - \omega$, and SST $k - \omega$ turbulence models [15]. The Reynolds stress can be obtained by solving the Reynolds Stress Model (RSM) with the predicted eddy viscosity. According to the Fluent User Manual (2003), it is possible to conclude some trusted predictions with the turbulence models of standard $k - \varepsilon$, RNG $k - \varepsilon$, and the standard $k - \omega$. The Fluent Tutorial (2004) [15] developed an investigation of a propeller flow field on the behavior of RNG $k - \varepsilon$ model and standard $k - \omega$ model, with a comparison of the measurement of realistic results.

2.5.1 Standard $k - \varepsilon$ Turbulence Model

The standard $k - \varepsilon$ turbulence model (Launder and Spalding, 1972) is a well-constructed two-equation turbulence model to decide the turbulence velocity and length scales separately. It is assumed that production rate and the dissipation of the turbulent flow have to be in a state of balance with transferring energy when the model is applied [15].

The dissipation rate of the energy ε can be obtained by the estimation given by:

$$\varepsilon = \frac{k^{3/2}}{l} \quad (2-9)$$

Where k means the kinetic energy of the flow and l is the involved length scale.

k is determined by the turbulent viscosity μ_t which is based on Prandtl mixing length model shown in the equation below [15].

$$\mu_t = \rho C_\mu \frac{k^2}{\varepsilon} \quad (2-10)$$

Where ρ is the density of the flow, and C_μ is an empirical constant.

The standard $k - \varepsilon$ turbulence model has been used in a wide range of turbulent flows but with some drawbacks in the predictions of the turbulence close to the stagnation point. It cannot

solve problems on large strains of the flows, which is usually covered in the field of swirling flows and curved boundary layers flows [15].

By applying statistical methods into standard $k-\varepsilon$ models, the standard $k-\varepsilon$ model can be improved with a new model named renormalization group theory (RNG).

2.5.2 RNG $k-\varepsilon$ Turbulence model

Choudhury [16] proposed a new statistical mechanics method called renormalization group theory to modify the standard $k-\varepsilon$ turbulence model. The small scales of motions are removed from the governing equations. Instead, the large scales of motions and a modified viscosity are implemented to express their effects [17].

2.5.3 Realizable $k-\varepsilon$ Turbulence Model

In order to satisfy the requirements of the Reynolds stresses, a mathematical method for improving the consistency of the flow is applied to solve problems especially with rotation and boundary conditions [15] and [18].

2.5.4 Standard $k-\omega$ Turbulence Model

In order to overcome the drawbacks of the standard $k-\varepsilon$ turbulence model near walls, Wilcox [19] proposed a standard $k-\omega$ model to deal with these terms. The standard $k-\varepsilon$ turbulence model is usually used into the cases with high Reynolds number. However, the Reynolds number along the wall is always low that it cannot satisfy the requirement of the standard $k-\varepsilon$ model. With modifications of the standard $k-\varepsilon$ turbulence model, a free shear flow can be calculated by the application of the standard $k-\omega$ turbulence model.

2.5.5 Shear Stress Transport (SST) $k-\omega$ Model

The shear stress transport is given by Menter [20] in 1994 which consists of the features of high and low Reynolds number from the standard $k-\varepsilon$ turbulence model and the standard $k-\omega$ turbulence model. As it is mentioned above, the standard $k-\varepsilon$ turbulence model can accurately predict the far field while the standard $k-\omega$ turbulence model can calculate the spreading rate of the shear flow near the walls.

F_1 is blending function which be switched into zero and one to represent the two models. It can be conclude with a new expression corresponding constants of the $k - \varepsilon$ model and the $k - \omega$ model described below [21].

$$\alpha = \alpha_1 F_1 + \alpha_2 (1 - F_1) \quad (2-11)$$

Where α_1 is the $k - \omega$ model, α_2 is the $k - \varepsilon$ model.

When F_1 is one, it will be switched to the $k - \omega$ model, on the other side, when F_1 is zero, the model will be switched to the $k - \varepsilon$ model.

Chapter 3 Methodology and FEM Analysis

The main and first challenge of the comparison for different designed models is a matter of making a good mesh. The main reason for this is that, despite being, generally, more elements generated and smoother growth for the grids on the propeller models preferred, the mesh for the models is quite significant to control the number of the elements under some limitation in order to reduce the computing time for the next analysis step, while providing a reliable and trustable grids. The mesh method will be introduced in this chapter, including the settings for the inflations, face sizing, contact sizing, body sizing, and the growth rate.

Geometries design from Nodin Innovation will be reported, together with an optimal mesh chosen for these models considering about the accuracy and simulation time. Moreover, setting up details will be mentioned, whose application is important to the boundary conditions and the realistic working environment for the propellers.

3.1 Geometry Description

Nodin Innovation designed different kinds of geometries for the propellers. Depending on the hub geometries and structures, the propeller models are named like Convex propeller, Concave propeller, Dome propeller, Center propeller, and Torqeedo propeller. With a configuration of the winglet, there is one propeller named Winglet propeller.

3.1.1 Convex propeller (Reference Propeller)

Convex propellers have been commonly used in the market of the modern commercial ships' propellers. With this kind of propeller to be a reference, the approach to investigating performances among other propellers will be easy to compare. The geometry of the Convex propeller from Nodin Innovation is shown in Figure 3-1. The distance from the leading edge to the trailing edge is 178mm.

The hub geometry is with a structure of convex, leading a possibility to discuss with other geometries, such as the Concave propeller, the Dome propeller, and the Center propeller. Except the hub part and the winglet part, other dimensions applied into other propellers are the same as the Convex propeller's.

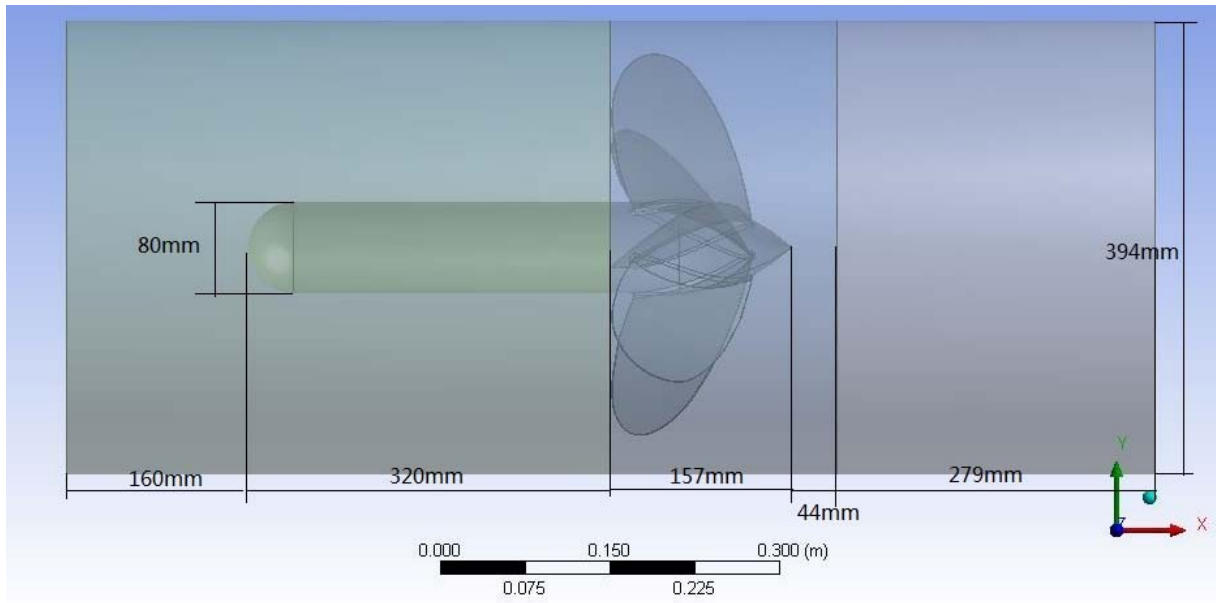


Figure 3-1 Geometry of Convex propeller

3.1.2 Concave propeller

The Concave propeller has the same design with the Convex propeller but the hub part. The 3-D model of the Concave propeller is shown in Figure 3-2 part a).

The hub with concave geometry will be expected to perform worse than the Convex propeller according to the experience with the raindrop geometries in the natural life [22].

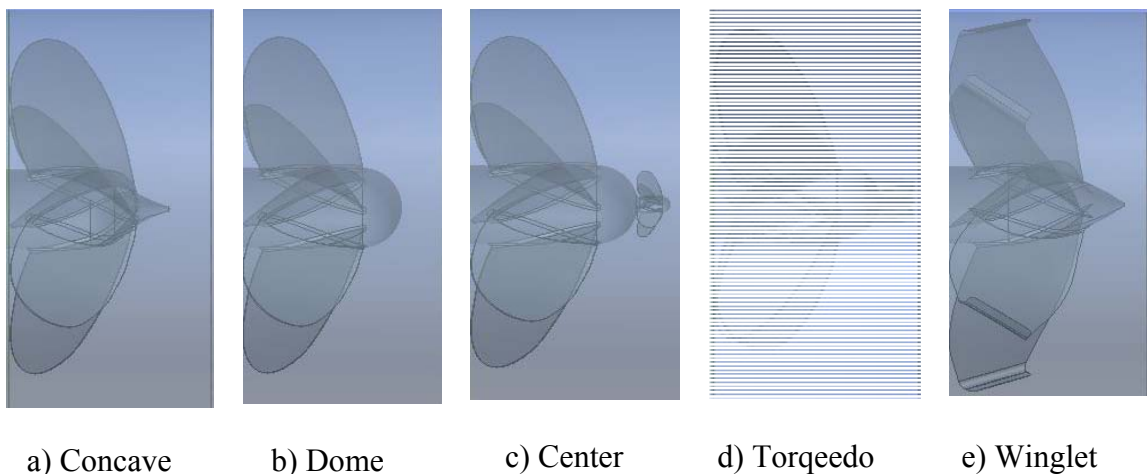


Figure 3-2 Geometries of propellers

3.1.3 **Dome propeller**

The Dome propeller has similar geometry like the design of the Convex propeller and the Concave propeller. However, the hub is implemented with a structure of dome. It is quite interesting to know the performances among the three propellers mentioned above, the different configurations of the hub impact on the thrust of the propellers with a prediction that the Dome propeller will perform the best and the Concave propeller will perform the worst in terms of the knowledge from the nature [22].

The 3-D geometry of the Dome propeller is shown Figure 3-2 part b).

3.1.4 **Center propeller**

The investigations into predicting the performances of different propellers are of particular interest for the hub geometries and the structure of the hub. A smaller center propeller is employed in front of the old hub to acquire the dynamic performances within the open water environment. In the fluent CFD investigation, the behavior of the configuration of the hub might lead to a considerable progress in velocity and thrust.

The design of a conventional propeller is the basis of the design of the propeller with a small Center propeller on it, as an alternative of the Center propeller, different geometries are encouraged to be tested. Here in this master thesis, it will only test the small Center propeller in the similar structure with the Dome propeller but in a tiny scale.

The geometry of the Center propeller is shown in Figure 3-2 part c).

3.1.5 **Torqueedo propeller**

The propeller configuration is playing a significant role in the dynamic performances. Optimization calculations have taken account of the effect of the propeller in turbulence flow. The Torqueedo propeller makes a new approach to avoid the turbulence in some level in order to provide a higher efficiency for the commercial ships [23].

The design of the Torqueedo propeller from Nodin Innovation consists of the most part of the Dome propeller and Torqueedo blades in front of the hub. The model is shown in Figure 3-2 d).

3.1.6 Winglet propeller

The winglets have already been applied into aircrafts for many years. It is reported that Boeing 737-800s with the split scimitar winglets should cut fuel cost by 2% which means the winglet structure will help save 200 million dollars [24].

Inspired by the data from Boeing 737-800s, the winglets for the blades of the propellers are expected to illustrate some better performances than the conventional propellers. The physical theory about the performance of the winglet is because the winglet curves are bended upward, leading a higher pressure on the lower surface of the wing. With this air force, the vortex is reduced which means the energy loss will be smaller.

The Winglet propeller from Nodin Innovation has the similar design with the Convex propeller except the blades with winglets. The hub part of the Winglet propeller is shown in Figure 3-2 e). Compared with the structure of the winglet on Boeing 737-800s, the Winglet propeller in this study has only the bended parts upwards.

It also has to be noticed that all the other parts of the propellers except the hub part are the same.

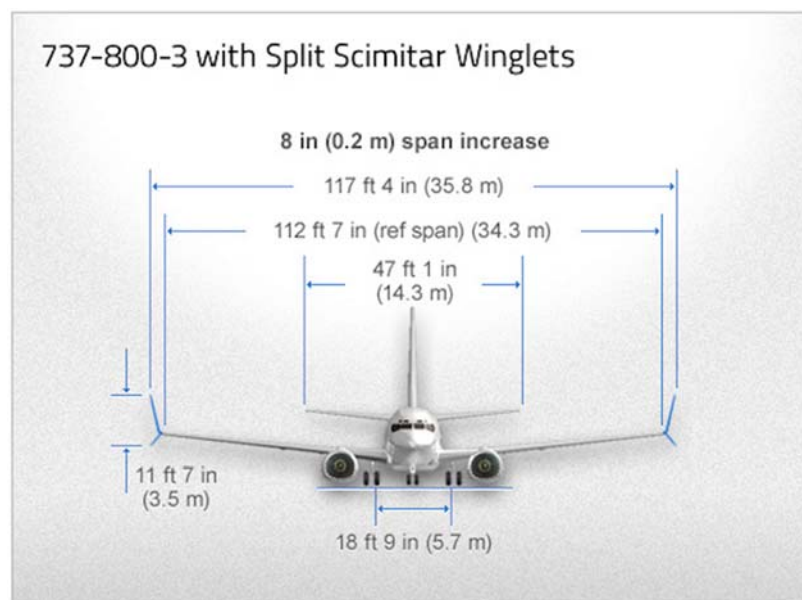


Figure 3-3 Boeing 737-700 with blended winglets

Picture is from the website [36]

3.2 Mesh

The generation of a suitable and fine grid is a crucial step in the simulation process [3]. Promoting the negligible error in the procedure of the simulation and reducing the computational time for the program are the main issues for generating the mesh. However, the process of generating grids can't reach the ideal conditions. The types of grid system available include unstructured (where no pattern is imposed on the distribution of points), Cartesian (where an unstructured pattern of squares is defined and the geometry cut out of this pattern) and Chimera (where overlapping meshes of a regular structure are used) [3].

There are two main methods to generate the mesh, one is to use the algebraic approach to make the grids, and the other one is to apply the partial differential equations to generate grids. In fact, the procedure for generating the grids is another way to do the mapping from the calculation plane to the algebraic plane. The structured grids are allowed to overlap, with a very efficient numerical process implemented on it. The unstructured grids have the advantages of the lack of restriction on where points can be placed, in other words, it means it is possible to provide an automation of generation with a high degree. However, the disadvantage of the unstructured grids is that they will cause the problems with a high level of anisotropy needed in the mesh, such as in boundary layers [3]. The mesh applied in these propeller models is the unstructured mesh which is also called the auto volume mesh, usually obtained after setting up all the parameters like inflations, the growth rate, the face sizing, the contact sizing, and the body sizing. This kind of mesh will reduce the cost of humanity but required a heavy work for the CPU of the computer. Therefore, reducing a very long computational time for each simulation is the basis issue of making mesh here.

The models of the propellers are 3-D models, so the three dimensional mesh are applied to the analysis of the 3-D models. The basic elements of the three dimensional meshes are the tetrahedron, quadrilateral pyramid, triangular prism, and hexahedron. The faces of these four

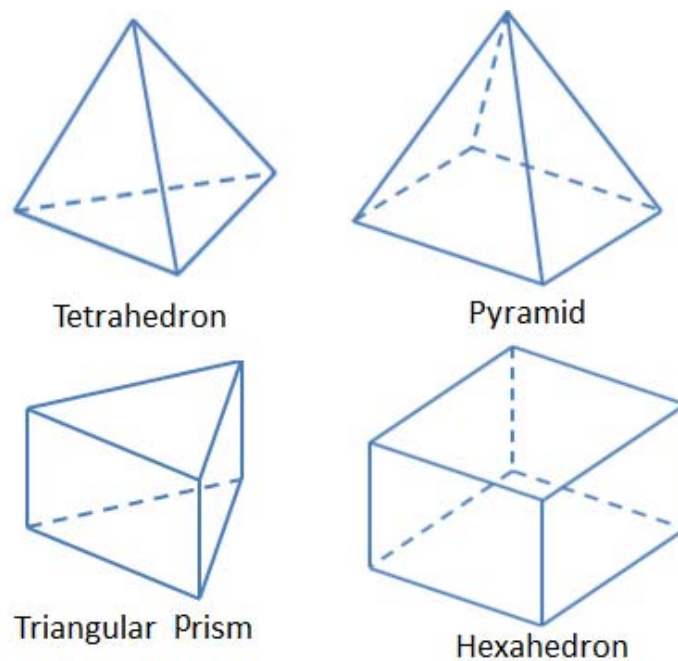


Figure 3-4 The basic elements of three dimensional cell shapes

which consist of the faces of triangle and quadrilaterals [25]

dimensional cells consist of the faces of triangles and quadrilaterals. The cells shapes of them are shown in Figure 3-4 [25].

The meshes for all the propeller models are applying the tetrahedron cell shape in this study. The tetrahedron cell shape has four vertices and six edges by four triangular faces which are shown above in Figure 3-4. Because we will not use other types of meshes in this report, other descriptions about types' descriptions of pyramid, triangular prism, and hexahedron can be found in [25].

3.3 Set-up of Mesh

For the best results of the mesh we can obtain, the parameterization of the mesh should be well behaved over the grids. This implies that the magnitude of the inflations, different sizing, on the parametric model surfaces and bodies should be taken account while doing the set-up, in order to get the fine mesh under the limitation of specific elements and nodes [26]. Since, in general, the mesh performed on the three dimensional models is expecting to behave in this manner. There are several mesh options listed in Table 3-1 to define the mesh for the propeller

Table 3-1 Mesh option and the positions

Mesh options	Position
Inflation	FaceA_house
Inflation	FaceB_propeller
Inflation	FaceB_tunnel
Inflation	FaceA_tunnel
Inflation	FaceC_tunnel
Face Sizing	FaceB_tips
Face Sizing	FaceB_connections
Contact Sizing	Interface AB
Contact Sizing	Interface BC
Body Sizing	Body A
Body Sizing	Body B
Body Sizing	Body C

model. A comprehensive and comparable of simulated data addressing the dynamic properties of the propellers is available for this fundamental step of a fine mesh.

In order to specify the positions in the model, the Convex propeller is chosen as the reference case and an example to show the details. The meaning for the name of the position can be understood in this way. FaceB_propeller means this locates on a face, in Domain B, and the propeller consists of three parts: blades, connections, and the tips. Regions of fluid flow and/or heat transfer in CFX are called domains. Fluid domains define a region of fluid flow with specified material in the region [27].

Table 3-2 Definitions of the face sizing of Convex propeller model

Position	Geometry	Type	Element Size(m)	Growth Rate
Tips	Body B	Element Size	0.0005	1.05
Connections	Body B	Element Size	0.005	1.05

3.3.1 Mesh options

3.3.1.1 Inflations

While the inflation is usually defined on the parametric space of the surface to give a smooth growth of the elements change. Three different inflations are proposed along three different faces. The details of the inflations are listed in the Table 3-3.

For this study, the inflations settings are used in the surface of the tunnel in A, B, and C domain, but the generated grids cannot be fine enough only with the settings of inflations. If no other sizing information is given, the elements number and the size for the mesh are too coarse to do

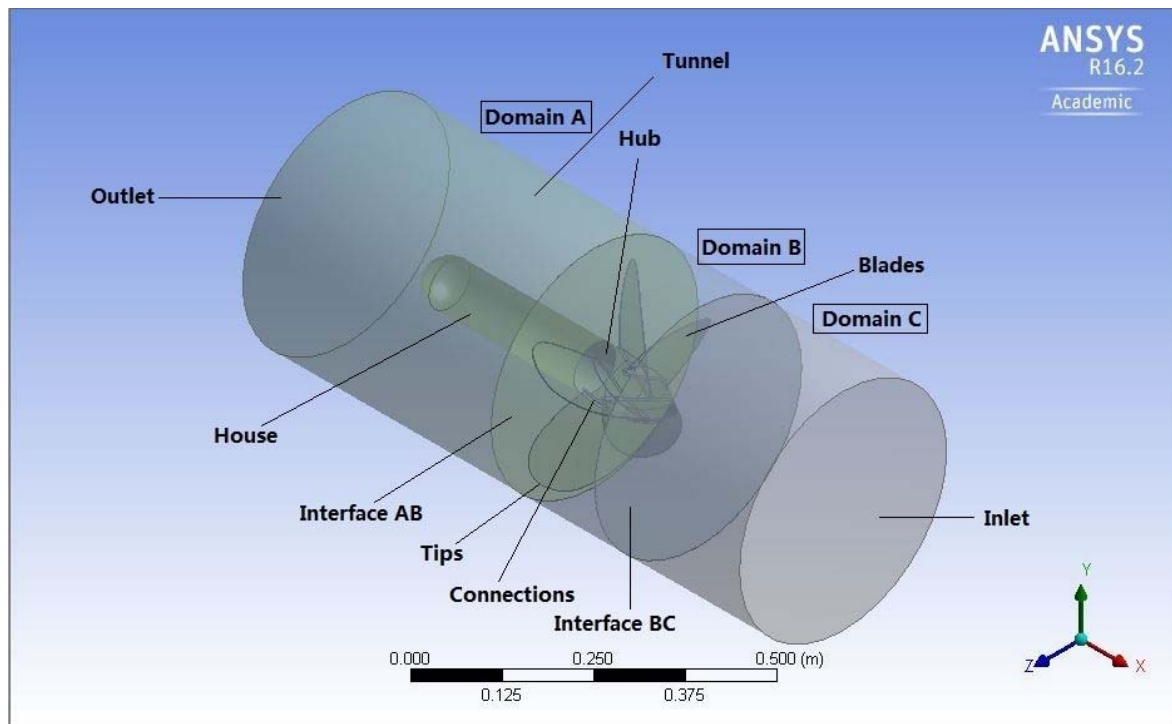


Figure 3-5 Positions and names of the Convex propeller

Table 3-3 Inflation options for the Convex propeller model

Boundary	Geometry	Inflation Option	Number of Layers	Growth Rate	Maximum Thickness(m)
FaceA_house	Body A	Total thickness	10	1.2	0.005
FaceB_propeller	Body B	Total thickness	10	1.2	0.005
FaceB_tunnel	Body B	Total thickness	10	1.2	0.01
FaceA_tunnel	Body A	Total thickness	10	1.2	0.05
FaceC_tunnel	Body C	Total thickness	10	1.2	0.05

an accurate analysis. This implies that the element sizes of the surfaces, the interfaces, and the body of the domain must be defined.

3.3.1.2 Face Sizing

Table 3-2 shows the details for the face sizing. Besides the face sizing for the tips and connections, the contact sizing of the interfaces will play a significant role for providing a smooth changes of the elements size from one domain to another domain.

3.3.1.3 Contact Sizing

The contacting sizing is specially implemented on the interfaces between the connecting domains, like Domain A and Domain B, and Domain B and Domain C. The definition details of the contact sizing are shown in Table 3-4.

3.3.1.4 Body Sizing

The rotating propeller is settled in the Domain B which requires more grids to describe the real geometries for the model. However, it is frustrating and time consuming to maintain the same amount elements for the stationary Domain A and C because there is not very complicated

Table 3-4 Definitions of contacting size

Contact Region	Type	Element size(m)
Domain A&B	Element size	0.007
Domain B&C	Element size	0.01

geometries in these two domains, even no geometry part of the propeller exists in Domain C. For this reason, different body sizes should be defined to achieve the desired size.

3.3.2 Mesh Statistics

Implemented with a slow transition of the changes of elements sizing, a smooth mesh along the propeller will be created. The more details for the mesh of the Convex propeller are shown in the Table 3-5.

3.3.3 Mesh results

The same mesh method is implemented into the Convex propeller, the Concave Propeller, the Dome propeller, and the Center propeller with a low rotating speed. When the Winglet propeller and the Torqeedo propeller use the mesh settings, because the structures of the two propellers and the limitation of the elements by the license, a different growth rate will be applied into all the propeller models except the Concave propeller with a high rotating speed.

3.3.3.1 Convex propeller

Figure 3-6 shows the glance of the whole mesh of the Convex propeller.

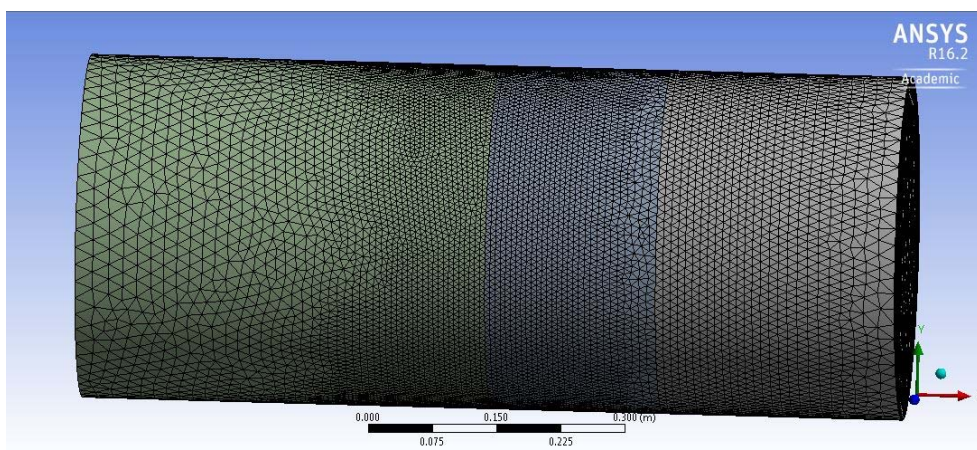


Figure 3-6 Mesh of the Convex propeller

The amount of the mesh grids of the Domain B is bigger than the other two domains. Make a cross section of the face XY, the details of the mesh are shown in Figure 3-7. Not only has the cross section of the Convex propeller showed the grids of Convex propeller, but the zoomed in inflation layers of the tunnels, and propellers have demonstrated that the proposed meshing method generates well-established grids. There is a smooth transition from Domain B to Domain A with slow growing of the grids. It will avoid a sudden change of the elements between the two domains.

Table 3-5 Mesh statistics for Convex propeller

Sizing Option			Inflation		
Use Advanced Size Function	On: Curvature		Use Inflation	Automatic	None
Relevance Center	Coarse		Transition Ratio		0.77
Initial Size Seed	Active Assembly		Maximum Layers		5
Smoothing	Medium		Growth Rate		1.2
Transition	Slow		Inflation Algorithm		Pre
Growth Rate	1.05		View Options	Advanced	No
Patch Independent Options			Patch Independent Options		
Triangle Mesher	Surface	Program Controlled	Topology Checking		No
Nodes		496 801	Elements		2 177 576
Min Size		0.00062606m	Max Face Size		0.05m
Min Edge Length		0.00021827	Max Size		0.05

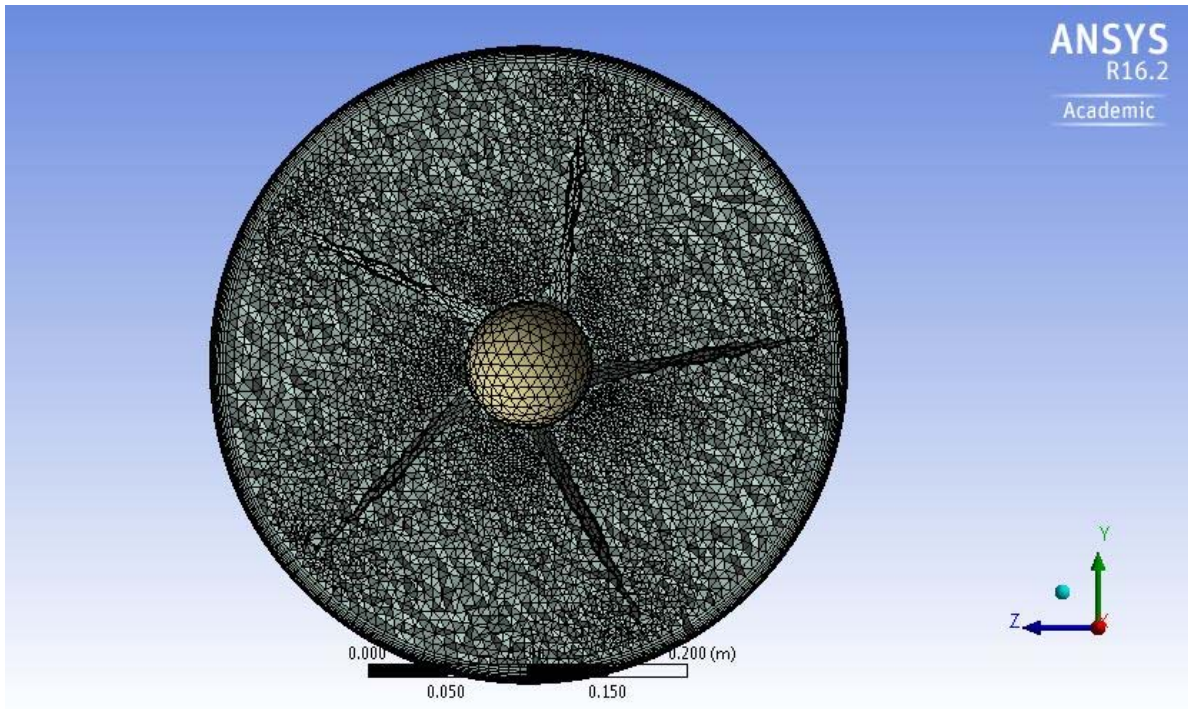


Figure 3-7 Cross section of the mesh of Convex propeller

The next issue to make sure the quality of the mesh achieve the requirement of the designs.

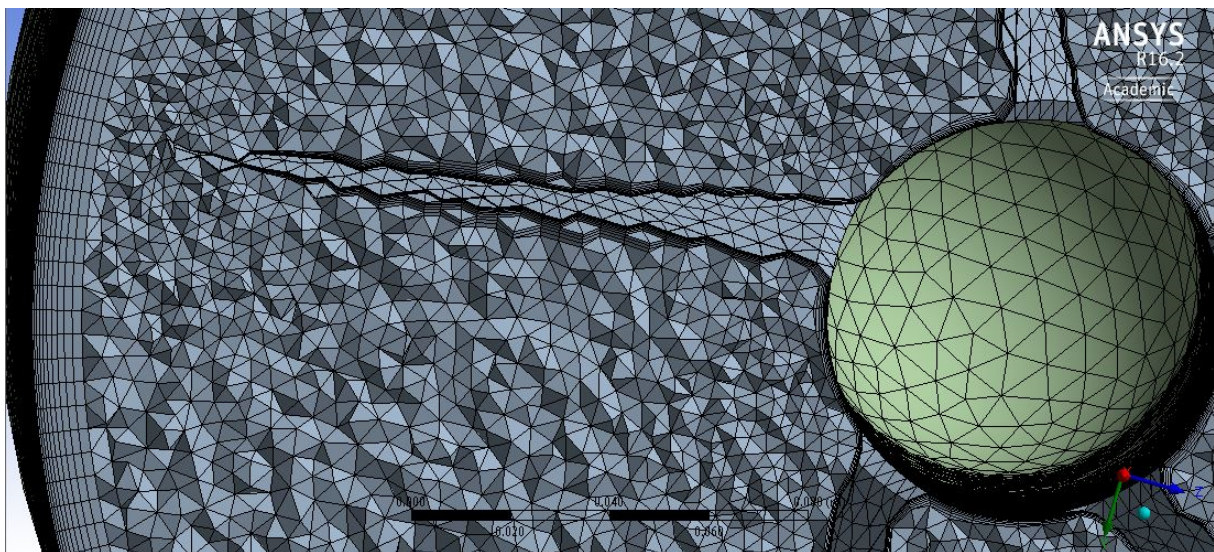


Figure 3-8 Zoomed in mesh of the blades, tips, and the tunnel of Convex propeller

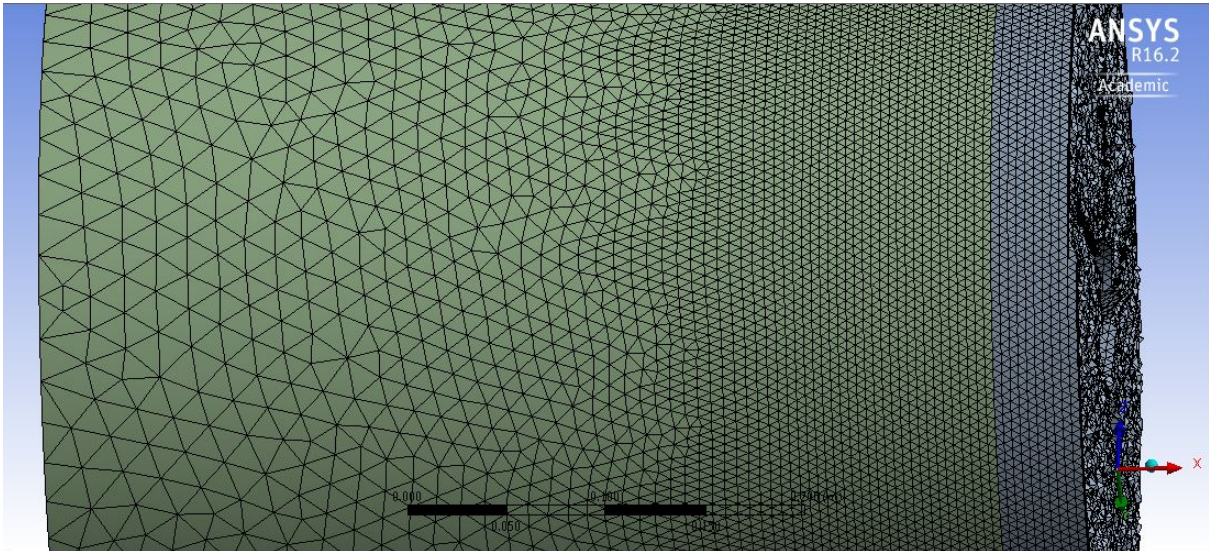


Figure 3-9 Mesh of the transition of Convex propeller between Domain A and Domain B

The quality of the mesh plays a significant role in the accuracy and the stability of the numerical computation. Checking the quality of the grids is the essential part while the different quality criteria are evaluated by the cell squish, and aspect ratio [28]. A suitable mesh is a balance between the mesh grids and the other three aspects.

First, a good mesh has to be possible to be computed. In other words, the computational time of the mesh has to be accepted during this project.

Second, a sound mesh needs to have very small elements in order to capture the physics of the models. For example, the elements size around the tips of the propeller has to be in a small scale to describe the geometry of the tips. If the elements size are too big, a distortion will be created there to lose the real geometry. Therefore, the settings of the inflation layers, the boundary layers are necessary to let the model stay in a trustable condition.

Finally, good mesh quality is significant.

To represent the details of the mesh quality results, Table 3-6 shows some numbers about the mesh metric.

Table 3-6 Statistic of mesh metric of Convex propeller

Mesh metric	Min	Max	Average	Standard Deviation
Skewness	6.1012×10^{-5}	1	0.21558	0.14846
Aspect Ratio	1.1616	284.83	2.969	4.9345
Element Quality	7.0416×10^{-3}	0.99997	0.7777	0.21151

From the results above, it is supposed to conclude this mesh is fine enough to our designs. The selection of the mesh options is required to apply to other propeller geometries in order to make comparisons.

3.3.3.2 Concave propeller

The comparisons of the dynamic properties are made by using the same mesh options applied to the designed propellers. Though it is impossible to provide the exactly same mesh for each geometry of the propellers. Implemented by the same settings of the mesh done like the Convex propeller, the mesh result of the Concave propeller is shown in Figure 3-10.

The inflation rate of 1.05 means the sizing elements of all the domains will follow this inflation rate to grow, however, the inflation rates from the mesh options of the surfaces are prior to be applied other than the inflation rate from the sizing options.

The details of the elements, nodes, and the inflation rate are shown in Table 3-7.

Table 3-8 Size statistic of the elements of Convex propeller

Min Size	Max Face Size	Max Size
0.00062606m	0.05m	0.05m

Table 3-7 Mesh statistics of the Concave propeller

Inflation rate	Nodes	Elements
1.05	438 216	1 829 755
1.06	392 938	1 593 712

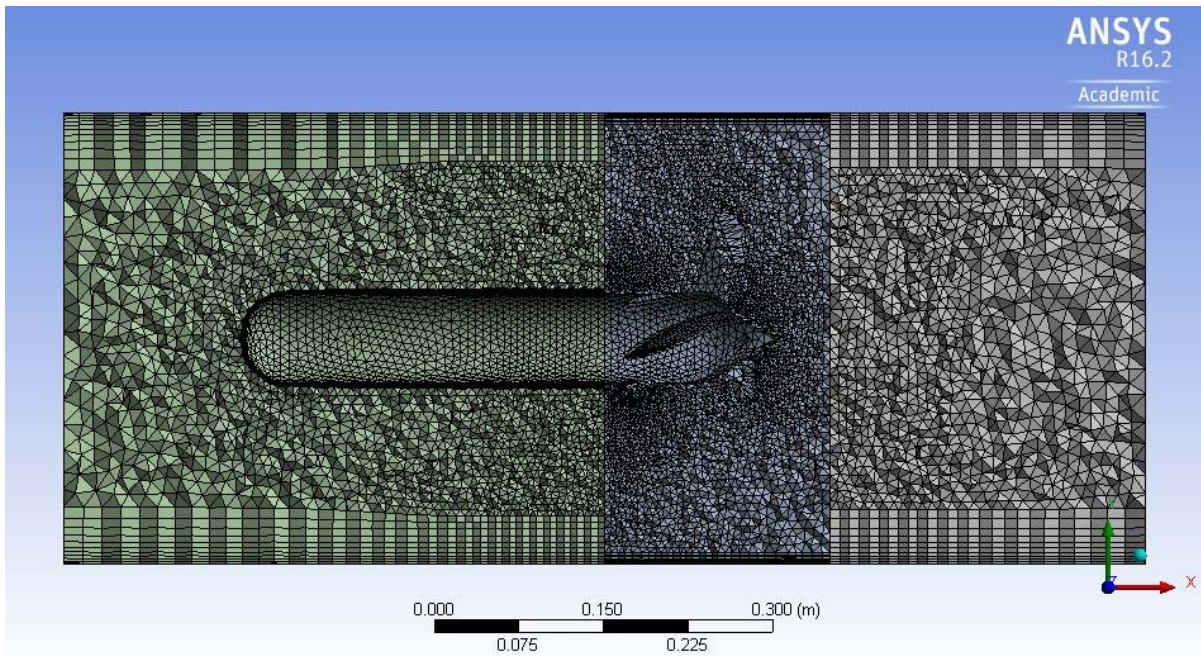


Figure 3-10 Cross section in XY plane of Concave propeller with inflation rate of 1.05

3.3.3.3 Dome propeller

To compare mesh results from different models, the same mesh options are proposed and applied. Mesh nodes, elements, and the cross section are available to show predicted mesh among all the models.

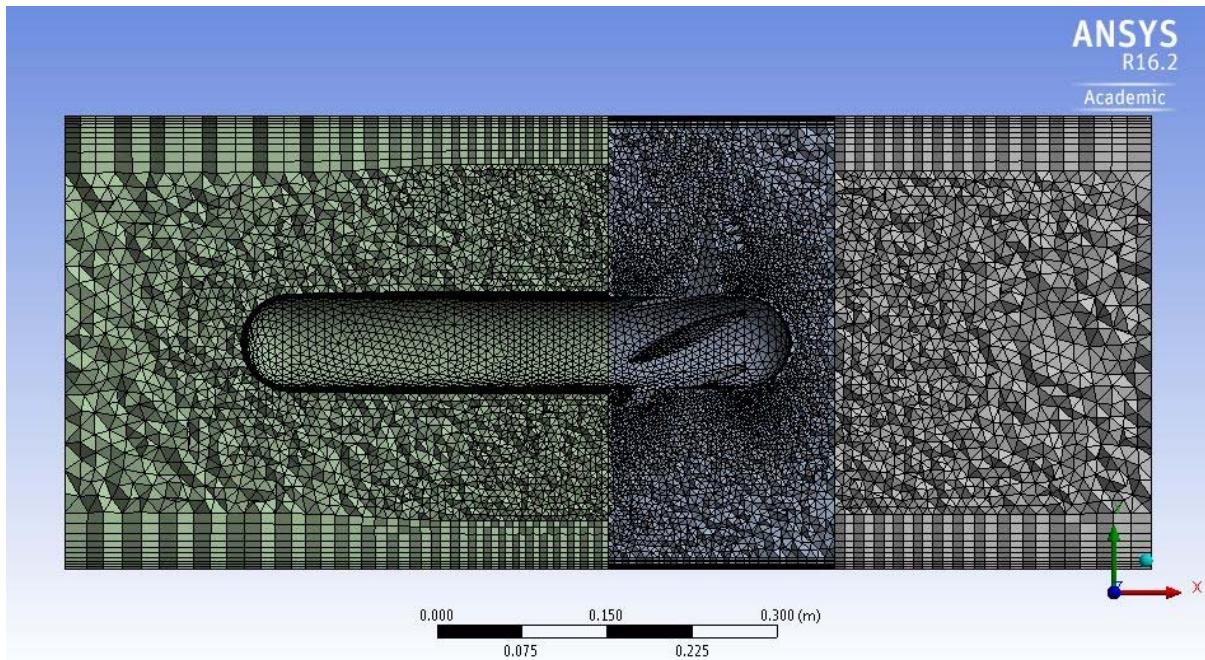


Figure 3-11 Cross section in XY plane of Dome propeller with inflation rate of 1.05

Table 3-9 Mesh statistics of Dome propeller

Inflation rate	Nodes	Elements
1.05	463 018	1 977 373
1.06	409 892	1 694 154

The details of the elements, nodes, and the inflation rate are shown in Table 3-9.

3.3.3.4 Center propeller

Because there is a small Center propeller located on the front to the hub, more elements will be generated. In order to follow the limitation of the student license, choose the inflation rate of the house of the propeller to be 0.05m instead of the old inflation rate along the house which has applied to other propeller models. Though there are some differences between them, it is impossible to provide all the mesh for the propellers with same amounts of nodes and elements due to the different geometries.

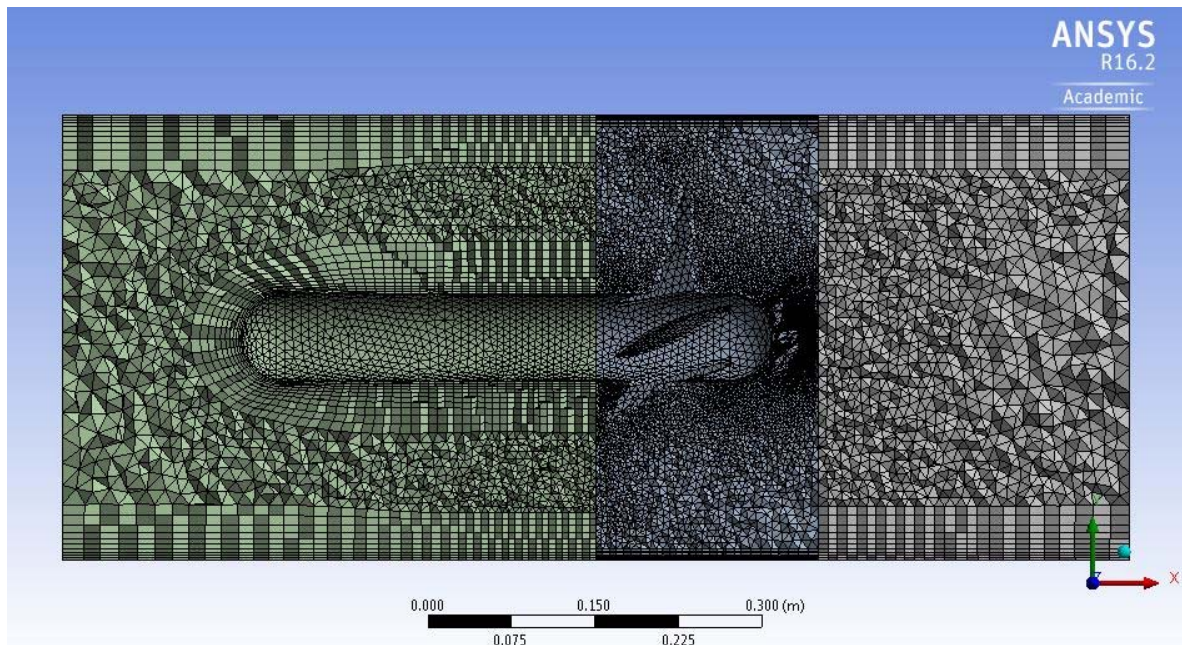


Figure 3-12 Cross section in XY plane of Center propeller with inflation rate of 1.05

Table 3-10 Mesh statistics of Center propeller

Inflation rate	Nodes	Elements
1.05	511 138	2 263 181
1.06	455 551	1 964 904

3.3.3.5 Torqeedo propeller

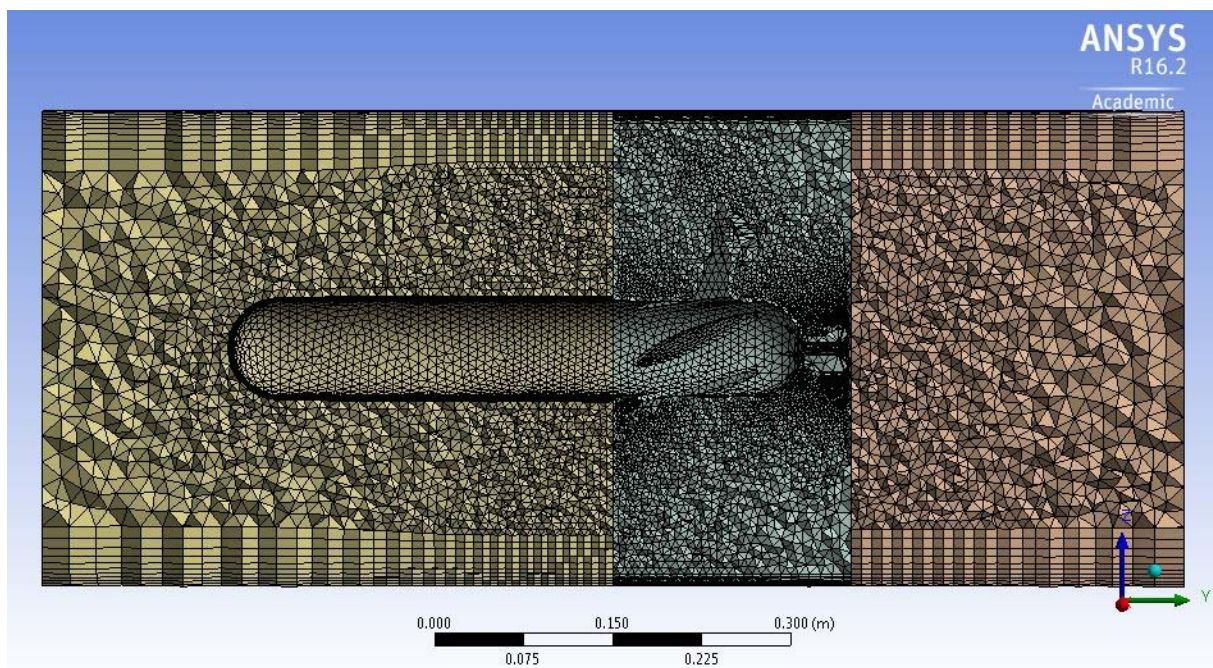


Figure 3-13 Cross section in YZ plane of Torqeedo propeller with inflation rate of 1.06

The details of the elements are shown in Table 3-11. The Torqeedo propeller has the same hub structure like the Dome propeller does. There are eight small blades on the front of the hub part. For the length from the peak position of the blade till the root part connect with the hub, it is 47mm.

Table 3-11 Mesh statistics of Toqeedo propeller

Inflation rate	Nodes	Elements
1.06	437 492	1 857 951

3.3.3.6 Winglet propeller

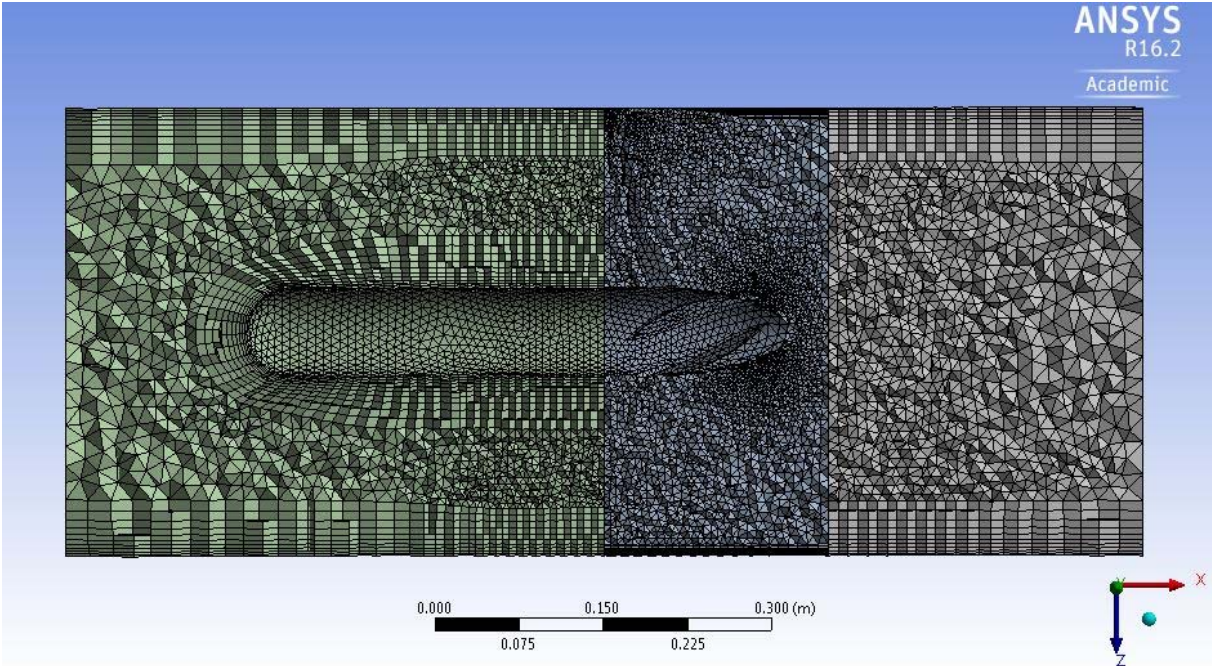


Figure 3-14 Cross section in XZ plane of Winglet propeller with inflation rate of 1.06

The details of the elements are shown in Table 3-12 .

With the limitation of the fluid physics of 521000 nodes in terms of the student license of ANSYS applied in this study, the inflation rate of 1.05 of the mesh option will lead more element nodes for the Torqeedo propeller. The computational mesh set-ups thus are adjusted to achieve the requirement of the student license with a bigger inflation rate of 1.06 used on Torqeedo propeller and Winglet propeller solved by SST model. Details will be describe in the Chapter 4.

Table 3-12 Mesh statistics of Winglet propeller

Inflation rate	Nodes	Elements
1.06	380 443	1 541 158

3.4 Set-up in Analysis Part

Three domains have been defined which is shown in Figure 3-5.

Domain A and Domain C are the stationary domains and Domain B is a rotating domain due to the blades part of the propeller located in it. Analysis type is a transient mode herein. And initial time in the automatic with value option is chosen, started with time at zero second. Explanations about the chosen options are shown in the Analysis Type of Chapter 2. According to the definition of the Automatic with Value option in 3.5.2, the physical set-up of the initial time of this whole analysis will be faster to find the zero condition because the velocity of the propeller is zero at the beginning.

3.4.1 Stationary Domains

When the fluid flow goes through Domain C and reaches the interface BC, which is in contact with the rotating propeller, a growing velocity will be applied to the flow. Accelerated flow goes across the interface AB to pass the Domain A whereas the mass flow at outlet is obtained. In the two stationary domains (Domain A and Domain C), boundary conditions like the inflation layers and contacting sizing are imposed to provide an appropriate stationary environment.

3.4.1.1 Domain A

The house of the propeller is located in Domain A. Without any rotation of the house, the flow which comes from the inlet through the rotating domain will not be accelerated again in Domain A. It is assumed that the continuous fluid is performed on the overall of the three domains.

Table 3-13 Setting options of Domain A

Boundary	Basic Setting	Boundary Details
FaceA_house	Wall	No Slip Wall/Smooth
Outlet	Opening	Static Pres. And Dirn
FaceA_tunnel	Wall	Free Slip Wall
Interface AB	Conservative Interface Flux	

Table 3-14 Setting options of Domain C

Boundary	Basic Setting	Boundary Details
Inlet	Opening	Static Pres. And Dirn
FaceC_tunnel	Wall	Free Slip Wall
Interface BC	Conservative Interface Flux	

This manipulation of the boundaries settings has a significant impact on the performance of the propeller. For Domain A, four boundaries have been modified based on the physics reality shown in Table 3-13.

In reality, there is no wall around the propeller when it is working in the ocean or the lake. The main goal of setting the walls for the propeller is to establish a working domain permitting the fluid flow to pass through within a specific field. Considering the real situation when the propeller operated on the commercial ships or the leisure boats, the tunnel of the Domain A is required to move freely with the water due to the nonexistence of the wall. A slip and smooth wall applied to the house part plays a similar role with the working fluid, allowing them go through this domain without unnecessary resistance.

The interface AB is the plane between Domain A and the Rotating Domain defined to be the general connection with the frozen rotor. Details about the interface definitions and settings can be found in 3.5.3 and 3.5.4.

3.4.1.2 Domain C

The Domain C has a similar setting with the Domain A due to their stationary property. The implementation of this domain offers an enough space of the fluid flow starting to be influenced by the motion of the rotating propeller. Setting details can be found in Table 3-14.

3.4.2 Rotating Domain

As implemented in Domain A and Domain C, the setting options are similar to the rotating domain. The propeller consists of the blades, the tips, the hub, and the house, which is shown

in Figure 3-5. A rotating function is carried out in the rotating domain to force the propeller in an appropriate performance.

$$V_{angular} = Ramp \cdot RPM \tag{4-1}$$

$V_{angular}$ refers to the angular velocity.

Details about the set-up options about the rotating Domain Are shown in Table 3-15.

In case of large rotation rates at the beginning, a Ramp function is defined as shown below.

$$Ramp = 1 - e^{(-t/0.1[s])} \tag{4-2}$$

The plot of the Ramp function is shown in Figure 3-15.

The implemented Ramp function roughly represents that after 0.5s, the propeller will be fully worked, and the velocity will still grow.

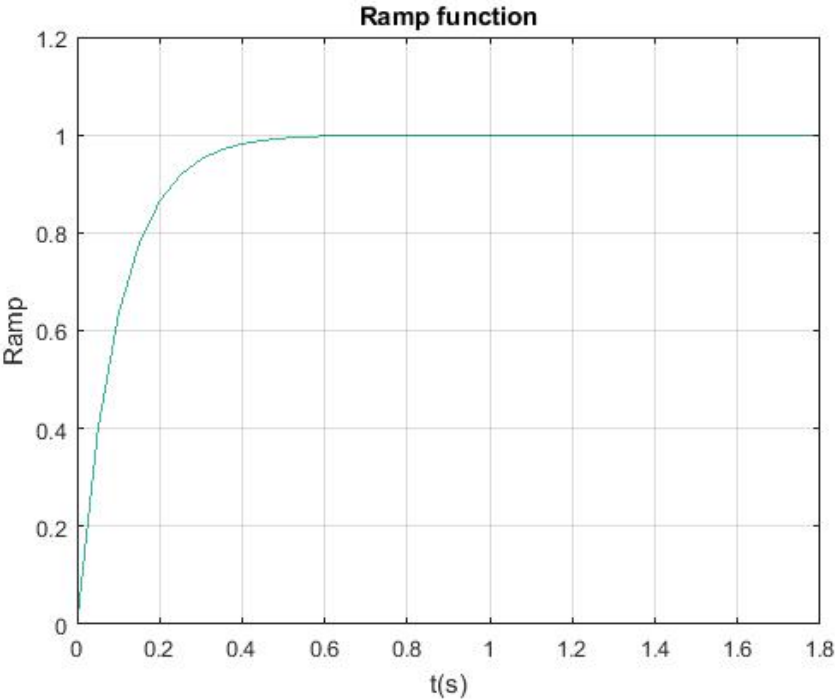


Figure 3-15 Ramp function

Table 3-15 Setting options of Domain B

Boundary	Basic Setting	Boundary Details
FaceB_propeller	Wall (Rotating)	No Slip Wall/Smooth
FaceB_tunnel	Wall (Rotating)	Free Slip Wall
Interface AB	Conservative Interface Flux	
Interface BC	Conservative Interface Flux	

3.4.3 Initialization

There are *Automatic* and *Automatic with Value* two options in the initial conditions in CFX-Pre settings. Global initialization options apply to the three domains in the simulations [27]. *Automatic with Value* enables the CFX-solver to automatically read the condition from an initial values file if it can find one, or else use the specified value or expression. As it is described before, at the start of the simulation, the propeller is stable with no velocity generated from it. The defined specific value, zero, of the velocities in three directions will be applied to the model with a faster achievement to find the initial condition. The global settings are shown below.

Table 3-16 Global settings regarding initialization

Frame Type	Stationary
Velocity Type	Cartesian
U	0 m/s
V	0 m/s
W	0 m/s
Relative Pressure	0 Pa

3.5 Analysis Type

3.5.1 Transient

Three available time dependences of the flow characteristics in ANSYS can be specified as the *steady state*, the *transient*, or the *transient blade row* [27]. Steady state simulations, by definition, are those whose characteristics are not in a linkage with the time and whose steady conditions are under an assumption that they have been reached after a relatively long time interval. Thus, the steady state requires no real time information to describe it. What's more, many practical flows can achieve the assumption that after initial unsteady flow development, they can be steady [27].

Transient simulation of the flow characteristics motivated by the real time information determines the time intervals at which CFX solver calculates the flow field. The initially changing boundary conditions of the fluid flows can influence the transient behavior. In addition, even all the other aspects of the flow conditions remain the same, a steady state condition is impossible to established here [27]. Because there is no resistance in the model of these propellers, the steady state condition will never be satisfied here, the transient mode is chosen to analyze the dynamic properties of designed models.

3.5.2 Initial Time

There are two options (*Automatic* and *Automatic with value*) available in this initial condition settings in CFX. Only solved or principal variable are initialized. If an initial field is required from other variables, it is derived from the solved variable initial fields [27]. The Automatic with Value option leads an avenue for the CFX solver to automatically read the initial conditions from an initial values files when they can find one initial condition with a value. Another condition is that this option is possible to use some specific expression.

3.5.3 Interface Models

The three available interface models consist of *Translational Periodicity*, *Rotational Periodicity*, and *General Connection*. The General Connection interface model is applied to connect regions together, especially in the condition with a change between the rotor and the stator. It is also available to link the surfaces with non-matching grids [27]. In order to reduce the computational time, the inflation rates of the tunnels in the stationary domains and in the

rotating domain are different that they can cause a difference of the grids in the faces connected with each domain. The general connection interface model is applied in the settings of Interface AB and Interface BC.

3.5.4 Frame Change/Mixing Model

There are three types of frame change/mixing models available in ANSYS CFX:

- Frozen Rotor
- Stage
- Transient Rotor-Stator

If we select None to be the option of the frame change/mixing model, it refers there is no frame change or pitch change in models. In the set-up, the Frozen Rotor is used in the propeller models as the propeller model has changed pitch and the frame of reference but the relative orientation of the components across the interface remains fixed [27]. The frames of the reference between Domain A and Domain B or Domain C and Domain B have a fixed relative position throughout the calculation. Accurate equation transformations are made with the changes of the frame as well as the fluxes are scaled with the changed pitch. More details and explanations about the Frozen Rotor can be found in [27].

Chapter 4 Results from Numerical Simulations

In this chapter, the turbulence models including the standard $k - \varepsilon$ and the shear stress transport turbulence model applied into the low and high RPM tests respectively in order to state the dynamic properties by making comparisons. For the purpose of the present study, it is appropriate to elaborate the differences of the mass flow through the interfaces, the inlet, and the outlet, to value the reference mass flow when the time-step is small enough to get a stable fluid flow. The numerical model is applied only on the propeller and there is no resistance from the vessel when it moves through water. In reality, the velocity of the propeller should grow until it achieves the balance with the resistance, however, in the model, the velocity will grow with no possibility to get balanced. Thus, it is convenient to monitor the mass flow explicitly as an option to determine whether the fluid flow is in a condition with the stability.

First, the time-step has to be decided on the Courant-Friedrichs-Lewy (CFL) criterion. Second, the reference number of the mass flow has to be found by using very small time step in a stable flow. With the difference between the reference number and the measured mass flow, it is possible to conclude the error and the range of application with these results. At last, compared mass flow can be checked to evaluate the performances of the propellers.

4.1 The Courant-Friedrichs-Lewy (CFL) criterion

The Courant-Friedrich-Lewy (CFL) criterion for the stability of numerical schemes is stated here, which is mathematically expressed in one dimension as [29]:

$$C_{FL} = \frac{u\Delta t}{\Delta x} < 1 \quad (4-1)$$

Where C_{FL} is the CFL number; u is the velocity of the local flow at the grid element; Δt and Δx are the temporal and spatial discretization respectively.

As pointed out in [33] and [32], it is commonly acknowledged not to be too small; in practice, as a rule of thumb, the CFL number is required to be as small as practically allowable [29].

When test the time-step for the model of Convex propeller under RPM of 100 rev/min, the absolute velocity in x direction of the standard frame at interface AB in ANSYS, the plane after the rotating propeller (details can be checked from Figure 3-5), is calculated to be 0.09409 m/s with a time-step set up to be 0.005s. From Table 3-8, the minim element size can be obtained, with a value of 0.00062606m.

Applying this data to formula (4-1) , the CFL number is given by:

$$C_{FL} = \frac{0.09409 \text{ m/s} \times 0.005 \text{ s}}{0.00062606 \text{ m}} = 0.751 < 1 \tag{4-2}$$

It is the purpose of the CFL number to show whether the time step used in the models is small enough or not. The CPU time of the Figure 4-1 is three days and eleven hours.

The velocity is growing but with a decreased part at accumulated time step of 300 to 500, details will be discussed in Chapter 5.

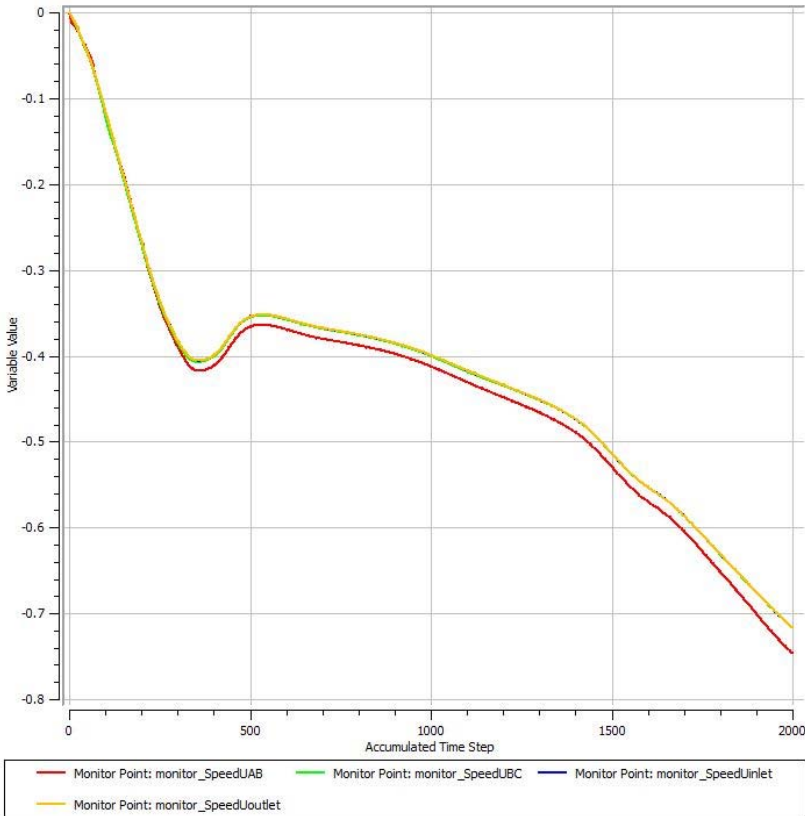


Figure 4-1 Monitored velocity in X direction of Convex propeller at RPM of 100rev/min with total time of 10s, and the time step of 0.005s

Nonetheless the total time of 10s and time-step of 0.005s will lead to a reference value of the mass flow, limited by the simulation time, it is necessary to figure out a relative proper total time and time-step with an error can be estimated to reduce the computational time.

4.2 Reference Number for Mass Flow of Convex propeller

The reference number can be found when the time step is very small and the flow is stable.

4.2.1 RPM of 100rev/min

The total time involves 0.5s, 1s, and 2s using a standard $k - \epsilon$ model with RPM of 100rev/min.

The first issue of relative importance is to find the proper total time to do the simulations of the propeller models. Coped with the Convex propeller chosen as the reference model for the tests, a series of simulations with different total time are implemented. The mass flow, the computational time (CPU) time, the differences of the mass flow through the inlet, outlet, and the interfaces have been monitored to conclude for a reasonable and reliable time-step and the total time. Results are shown in Figure 4-2.

The CPU time needed excludes the possibility of running all the simulations with the total time of 2s, 1s, and 0.5s and time-step smaller than 0.1s shown in Figure 4-2.

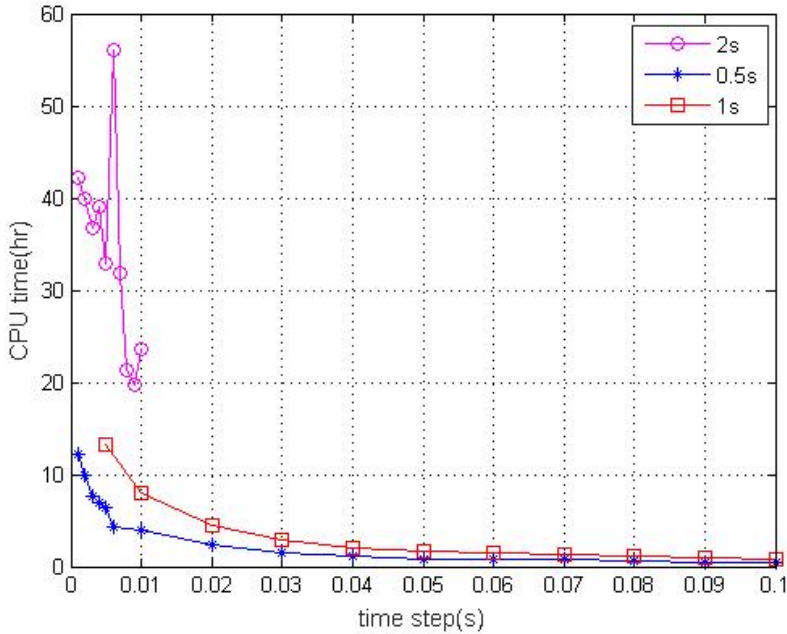


Figure 4-2 Time-step and CPU time with different total time

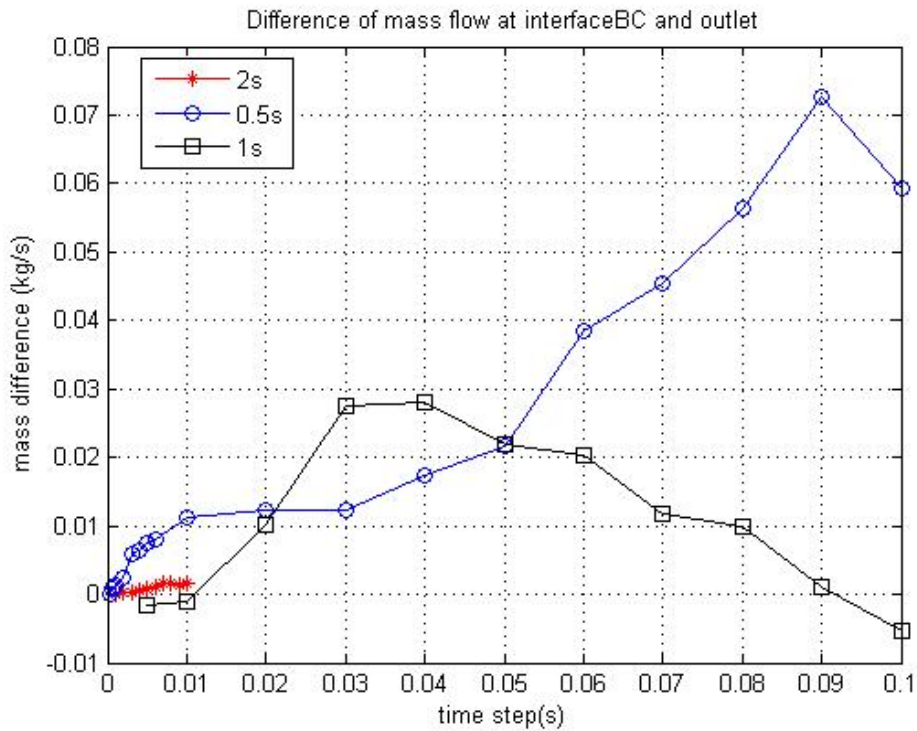


Figure 4-3 Difference of mass flow between interface BC and outlet

With a varied time-step applied into three different total time, the values of the mass flow at outlet are shown in Figure 4-4. Regression functions of the time step and the mass flow are listed below.

When the total time is 2s:

$$m = 192.55t + 48.75 \quad (4-3)$$

Here t represents the time-step in unit of second, m represents the mass flow in unit of kg/s through a cross-section of the outlet.

When the total time is 1s:

$$m = 58.78t + 33.33 \quad (4-4)$$

When the total time is 0.5s:

$$m = 56.65t + 14.23 \quad (4-5)$$

In Figure 4-2, the CPU time for the simulations with the total time of 2s is too long to be implemented for checking the performances of other propellers. Compared with the total time of 1s and the total time of 0.5s, after the time step of 0.03s, the CPU time is much shorter than

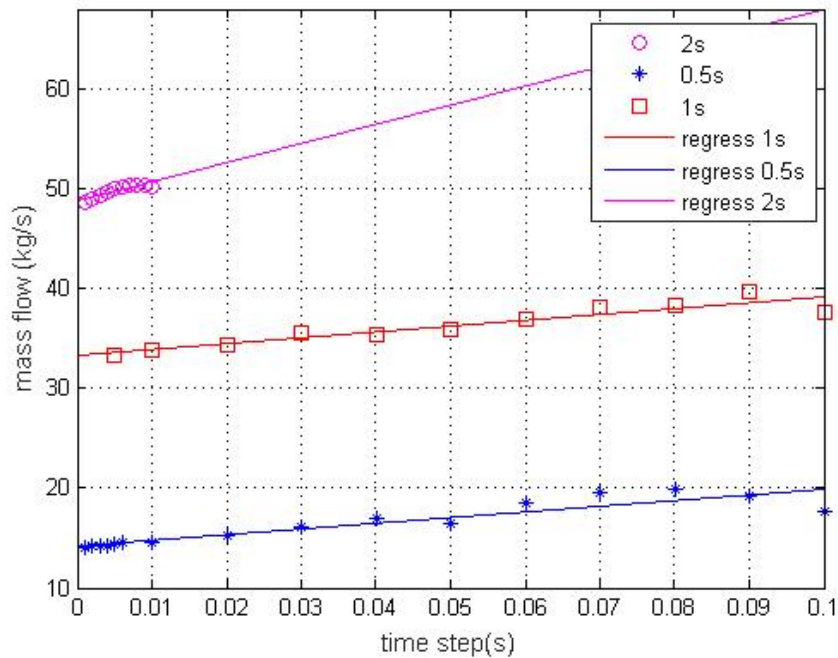


Figure 4-4 Different mass flow changed by time step within 2s, 1s, and 0.5s

before leading to a possibility to run all the simulations. According to the difference of the mass flow between interface BC and the outlet in Figure 4-3, the difference with the time step of 0.05s is acceptable. The gradients of the three regression lines are different because the velocities of propeller performed within the total time of 2s, 1s, and 0.5s are different. With no resistance from the vessel, the speed of the fluid flow is growing all the time. It is easy to understand that with a longer working time, the speed will be higher. From the Figure 4-4, when the time step is smaller than 0.01s, we have a very stable flow. The CPU time is too big to choose this time step. An obvious manifestation of the difference of the mass flow between interface BC and the outlet arises a suggestion for choosing the time step and the total time. Thus, the total time at PRM of 100rev/min is 1s and the time step is 0.05s. The reference value of the mass flow with total time of 1s is 33.3817kg/s when the time-step is 0.005s.

4.2.2 RPM of 3000rev/min

The same approach as in 4.2.1 is applied on RPM of 3000rev/min to give a suggestion of the time step. Total time of one second followed from the RPM of 100rev/min is applied here in terms of the computational time. The CPU time is always the issue we considered which has a linkage making this study possible in the given time frame.

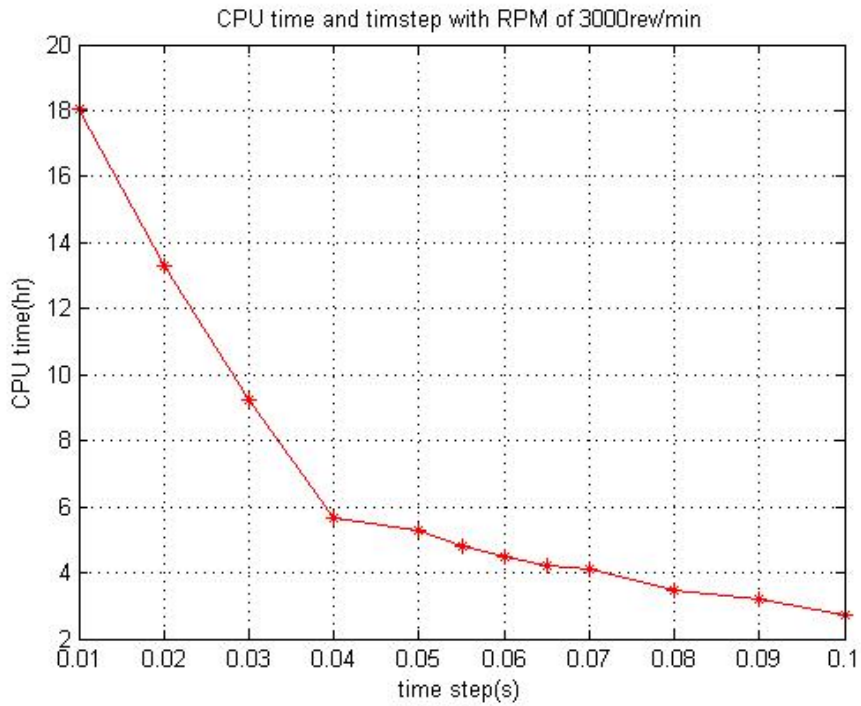


Figure 4-6 CPU time and time step with RPM of 3000rev/min

As thoroughly described in Figure 4-6, the CPU time has a big decrease after $\Delta t \geq 0.04s$. Another issue we consider about is the mass flow. In the Figure 4-5, it is shown that the mass

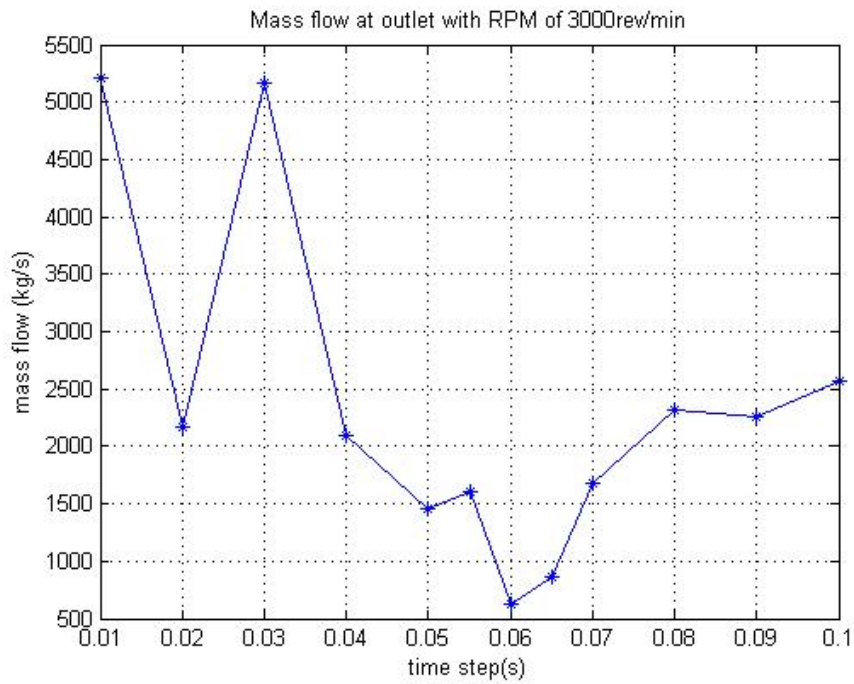


Figure 4-5 Mass flow at the outlet with RPM of 3000rev/min

flow at the outlet is not as stable as with RPM of 100 rev/min. It means a bigger time step used here result in instability of the flow. It is obviously better to make a smaller time step to run the simulation. However, considering the computational time, a proper time step has to be smaller than 0.01s which means that the computational time has to be longer than 18 hours.

With the instability with RPM of 3000rev/min, a guess with RPM of 1500rev/min is proposed to check whether a relative small RPM can have a stable condition.

4.2.3 RPM of 1500rev/min

Using method mentioned in 4.2.1, the proper total time and the time step are checked via an analysis of the computational time and the mass flow through the inlet, interface AB, interface BC, and the outlet.

The simulations carried out with the Convex propeller model still show the insatiability of the flow because the time step is not small enough according to the CFL criteria.

$$C_{FL} = \frac{15.04\text{ m/s} \times 0.05\text{ s}}{0.00062606\text{ m}} = 1201.16 > 1 \tag{4-6}$$

The computational time of the simulations are described in the Figure 4-7.

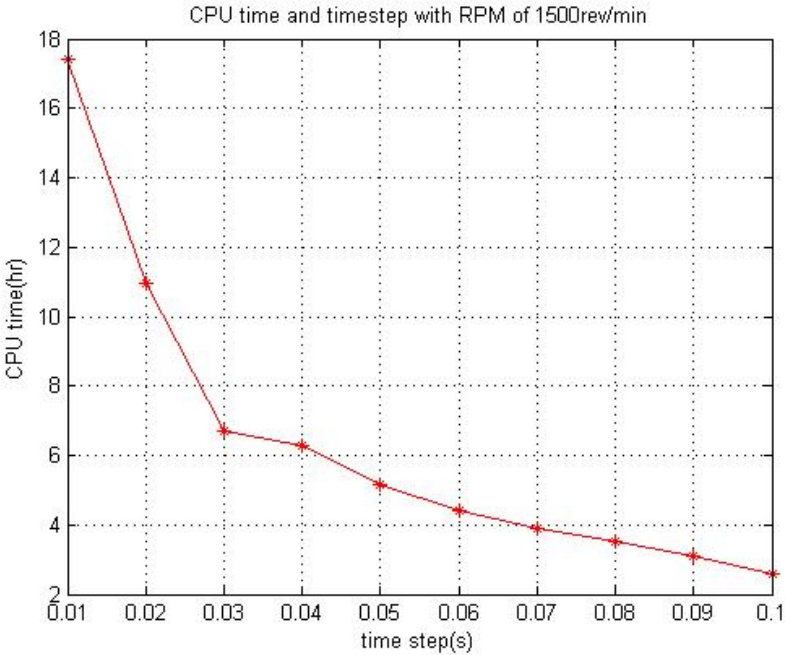


Figure 4-7 CPU time and time step with RPM of 1500rev/min

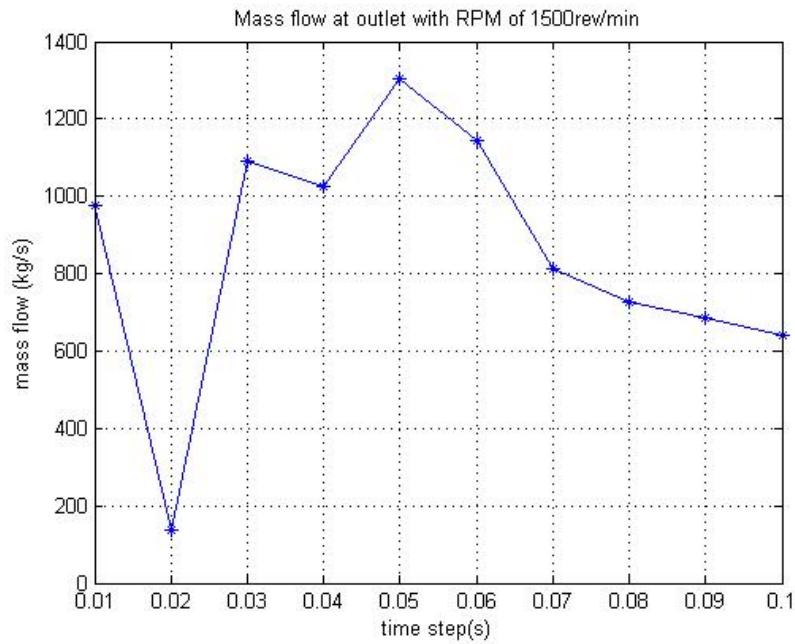


Figure 4-8 Mass flow at the outlet with RPM of 1500rev/min

The mass flow at the outlet is shown in the Figure 4-8. The data from Figure 4-7 and Figure 4-8 is used to choose an appropriate total time and the time step. Through the observation of the two figures, at the time step of 0.03s, the computational time get a sharp decrease with a mass flow around 1100kg/s, however, the mass flow changed with the time step affects the instability of the flow, even the time step is decreased to 0.01s, the flow is not achieving the stable condition. Details for the reference time step and total time will be discussed in 0. Due to the time limitation for this study, 0.05s is chosen to be the time step and 1s is decided to be the total time for all the simulations.

4.3 Different Propeller Models and RPMs

The chosen time step and the total time discussed in 4.2, are applied on the different propeller models with a range of RPMs.

Low speed (RPM less than 100rev/min) and high speed (RPM less than 3000rev/min, higher than 500rev/min) are applied. The present study consists of the two parts with different velocities of the rotating blades shown in the following subsections.

4.3.1 Comparison of Propellers with Low Speed

To maintain meaningful predictions and comparisons of the performances of the designed propellers, the same mesh, time step, and the total time are used to solve the mass flow through the surfaces along the models, in order to make relative mass flow to predict the behavior of propellers. The mass flow at outlet of the four propellers changed with RPM is shown in the Figure 4-9. These mass flow plots at the surface of outlet with the growing RPMs, can manifest propeller performances, mean that a higher speed of the blades will gain a bigger thrust and drag more water passing through the outlet. In order to compare other propellers' dynamic characteristics, a relative mass flow which represents the mass flow of a particular propeller over the mass flow of the Convex propeller at the same rotating speed is necessary in spotting the comparisons. Figure 4-10 shows the mass flow of the different propellers relative to the mass flow of the Convex propeller.

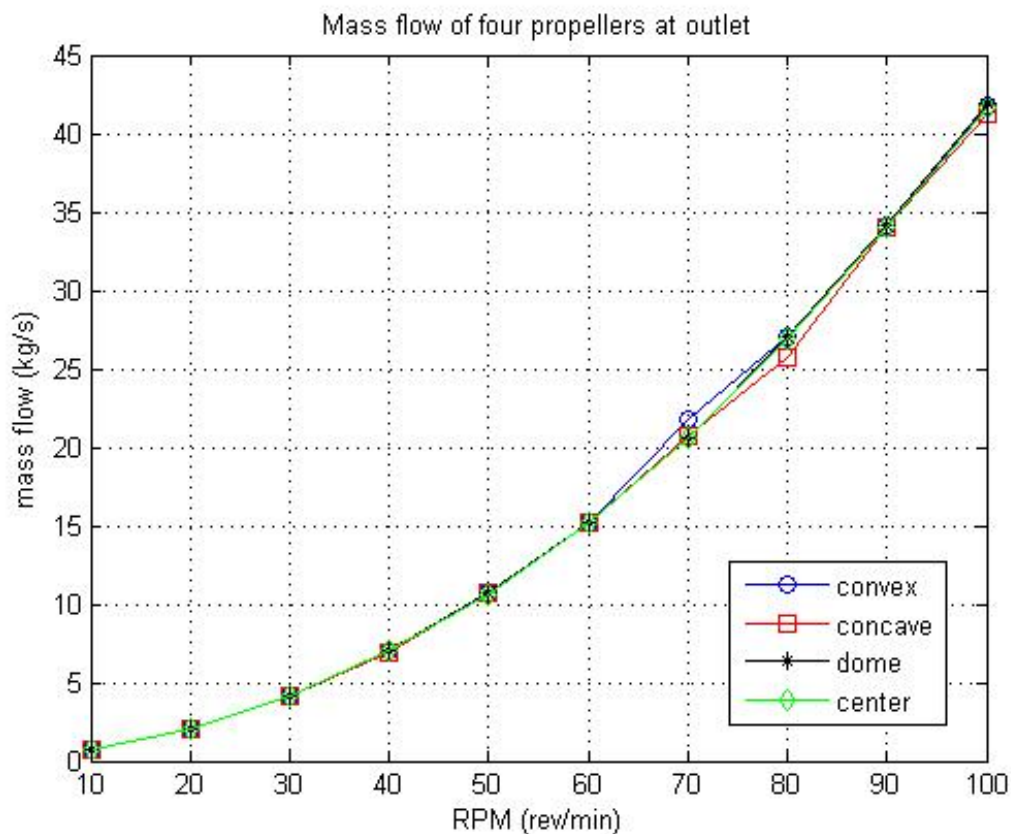


Figure 4-9 Mass flow at outlet as a function of RPM for four propellers

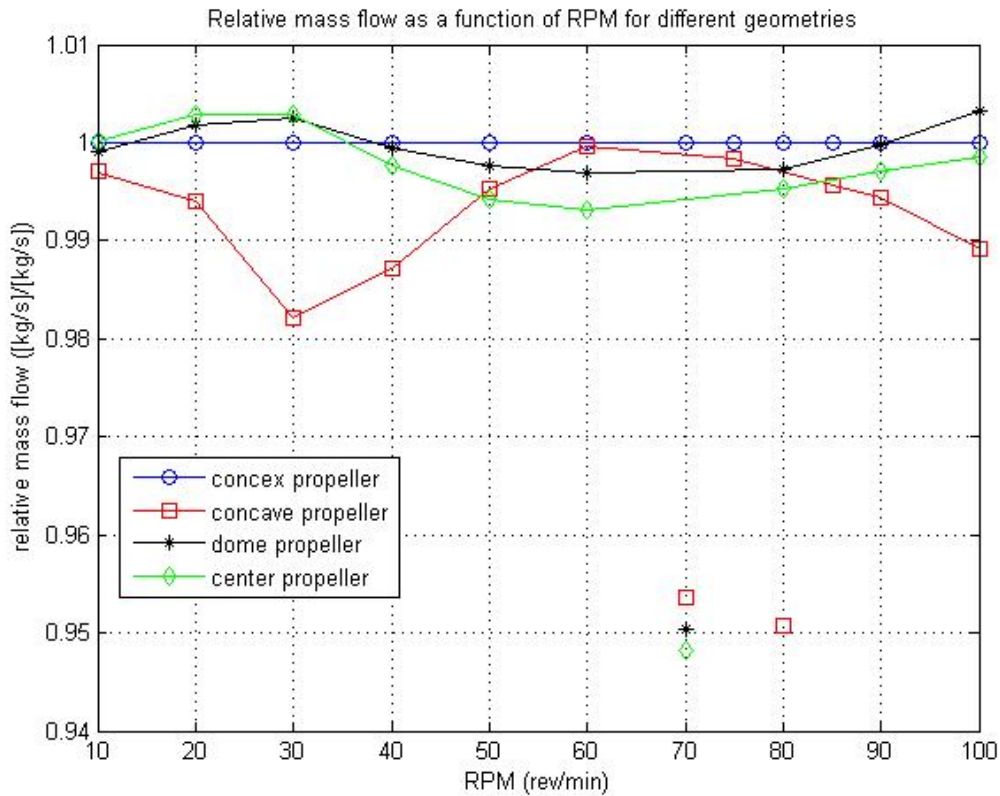


Figure 4-10 Relative mass flow as a function of RPM for different geometries

With the relative mass flow, it is more obvious to see which propeller has a better performance through the tendency of the lines. The observation of the mass flows at RPM of 70rev/min is far away from the others points, the grid sizes of the mesh may approach through the CFL criteria to the difference of the four kinds of propellers. At the same time, the tendency of the Concave propeller is not only unstable at RPM of 70rev/min, but also at RPM of 80rev/min. Simulation results reflect dynamic properties of the propellers with expectation. Various velocities are implemented in these ANSYS models showing a prediction that with a higher speed of the Dome propeller, a bigger thrust may be provided by the Dome propeller. All of these plots lead an interest to simulate the RPM with higher speed. From Figure 4-10, the Concave propeller performs worst among all the propellers. The mass flow is not in a stable line for Concave propeller no matter the RPM is low or high.

When the RPM changes from 10rev/min to 40rev/min, the Dome propeller and the Center propeller have a better performance than the Convex propeller. However, if the RPM grows a

little more till 90rev/min, it is obvious that the Convex propeller has a better performance. When the RPM reaches 100rev/min, the Dome propeller has the best performance in this RPM range.

4.3.2 Comparison of Propellers with High Speed

Computational models are briefly recalled here, whereas a high scale of the rotating speed applied into propellers are simulated and compared in this section. Considering the grids limitation of the Winglet propeller and the Torqeedo propeller, growth rate of 1.06 is implemented for accomplishing models through the sheer stress transport turbulence models.

Like the total time and the time step discussed in RPM of 3000rev/min in 4.2.2and 4.2.3, the results will be trusted but with errors due to the time step. For the RPM of 1500rev/min, the time step of 0.03s and total time of 1s are applied into the propellers. And the time step of 0.05s and total time of 1s are implemented into propellers with RPM of 1250rev/min, 1000rev/min, 750rev/min, and 500rev/min. In fact, the mass flow with RPM of 1500rev/min is also simulated within different propellers, which is shown in Figure 4-11.

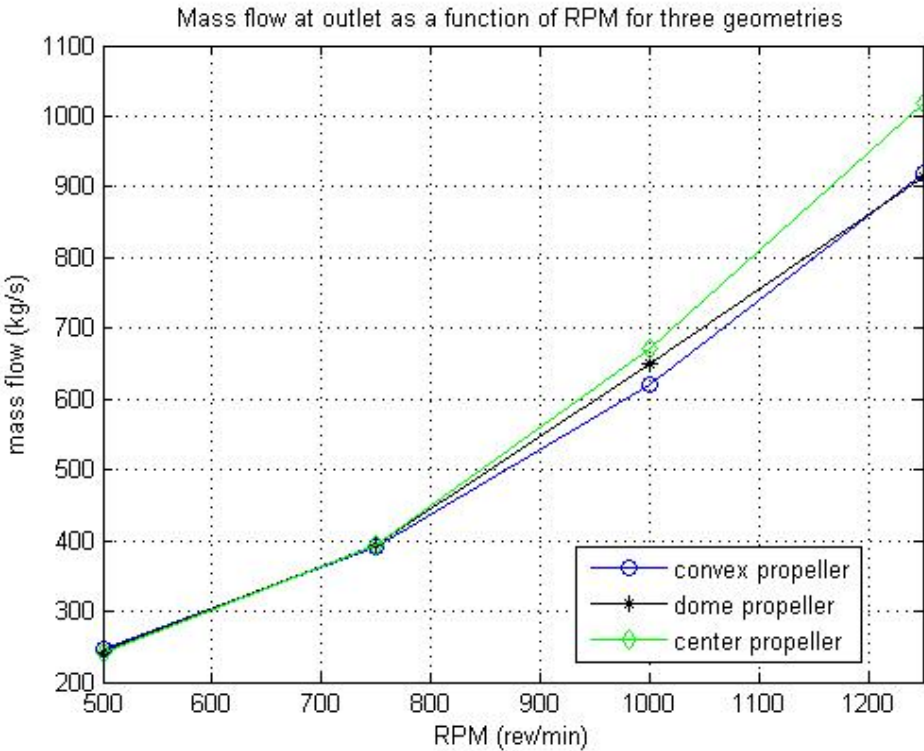


Figure 4-11 Mass flow at outlet and RPM of propellers

Table 4-1 Mass flow at Outlet with RPM of 1500 rev/min

Propeller Type	Mass flow at Outlet (kg/s)
Convex propeller	1092.46
Dome propeller	369.74
Center propeller	384.238

The mass flow with RPM of 1500rev/min in the Dome propeller and Center propeller is much smaller than the tendency of the lines predict in Figure 4-11. The monitor results of the velocities will be in shown in Figure 4-12 and Figure 4-13.

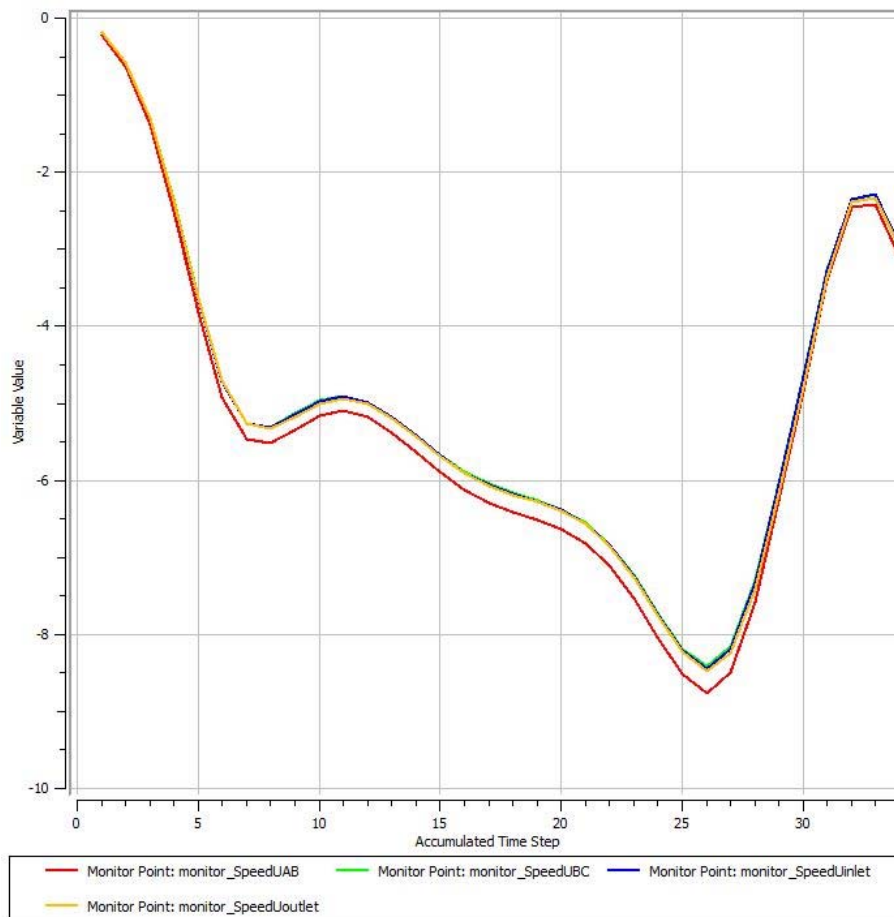


Figure 4-12 Monitor results of the whole simulation with the Dome propeller at RPM of 1500 rev/min within total time of 1s and the time step of 0.03s

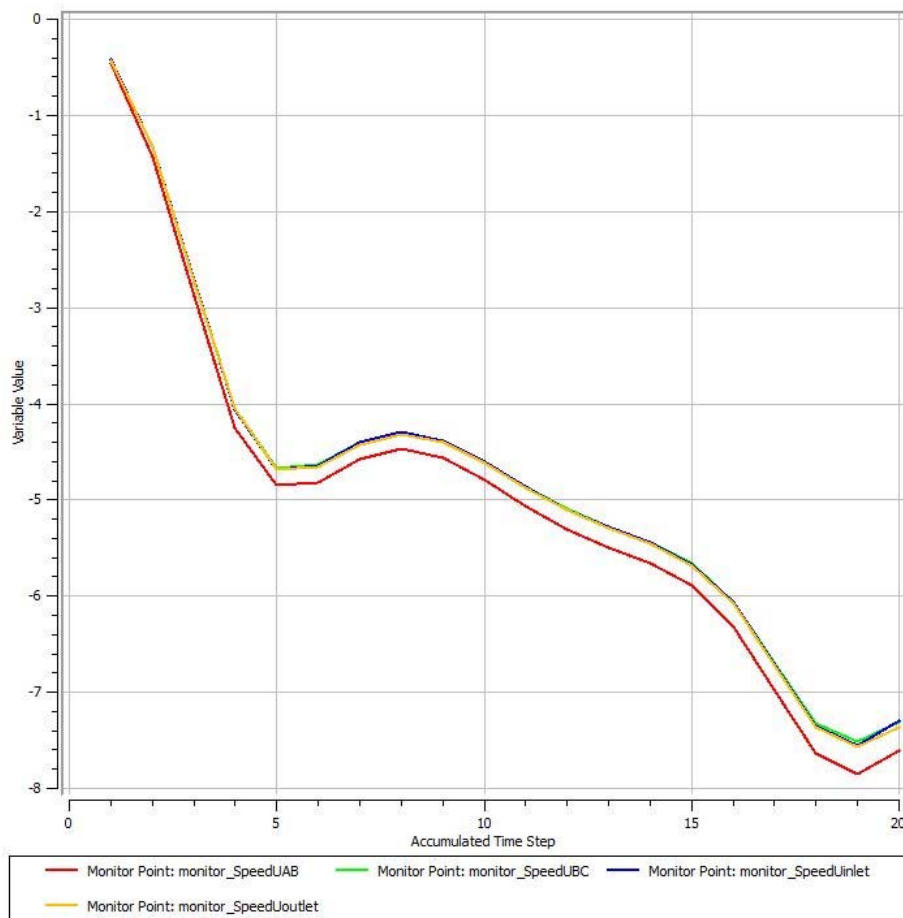


Figure 4-13 Monitor results of the whole simulation with the Dome propeller at RPM of 1250 rev/min within total time of 1s and the time step of 0.05s

Where:

SpeedUAB is the velocity in x direction when the flow passes through the interface AB.

SpeedUBC is the velocity in x direction when the flow passes through the interface BC.

SpeedUinlet is the velocity in x direction when the passes through the inlet.

SpeedUoutlet is the velocity in x direction when the passes through the outlet.

The Figure 4-13 presents an increasing tendency of the velocity roughly though there is a turning point referring to a decrease to the velocity. The comparison is obvious because the turning point appears at steps around of 26 within RPM of 1500 rev/min for the Dome propeller, which is earlier than the steps of 19 within RPM of 1250 rev/min. The two simulations' monitoring curves suggest that a smaller time step should be applied into these models.

Table 4-2 Mass flow and RPM for Winglet propeller

RPM	Mass flow at Inlet(kg/s)	Mass flow at Interface AB (kg/s)	Mass flow at Interface BC(kg/s)	Mass flow at Outlet(kg/s)
500	365.872	0.0455	4.0645	0.0451
750	476.577	0.0579	5.2976	0.0583
1000	649.048	0.0793	7.2097	0.0804
1250	915.857	0.1144	10.1797	0.1133
1500	664.934	0.085	7.3853	0.0829

When the Dome propeller rotates with RPM of 1500 rev/min, total time of 1s, and the time step of 0.03s, by monitoring the velocity at interface AB, the CFL can be calculated:

$$C_{FL} = \frac{21.30 \text{ m/s} \times 0.05 \text{ s}}{0.00062606 \text{ m}} = 1701.11 > 1 \quad (4-7)$$

When the Dome propeller rotates with RPM of 1250 rev/min, total time of 1s, and the time step of 0.05s, by monitoring the velocity at interface AB, we can get:

$$C_{FL} = \frac{12.26 \text{ m/s} \times 0.05 \text{ s}}{0.00062606 \text{ m}} = 979.14 > 1 \quad (4-8)$$

With the results of CFL, it is possible to conclude the time step applied into the two simulations shown in Figure 4-12 and Figure 4-13 is not small enough to let the flow reach the stability.

The mass flow results are not stable at all, details can be checked in Table 4-2.

According to the result in Figure 4-11, it seems that the Center propeller is able to provide a higher thrust but a smaller time step is necessary to make more simulations for accuracy in the future.

Chapter 5 Discussion

5.1 Compared Results of Propellers

The Concave propeller performs the worst among the four sorts of propellers, especially at the RPM of 30rev/min, and RPM of 80rev/min. Why the Concave propeller has a worse dynamic performances than others? First, it is wise to check the hub parts of those propellers.

From the Figure 5-1, it can be observed clearly there is a pointy part in the hub of the Concave propeller.

To determine the hub structure of the propellers, the observations that the shape of raindrops at their terminal velocity changes in a predictable manner with size has motivated numerous studies on the effects of raindrop shapes. Since the effective sizes of raindrops are correlated with rain rates with larger and thus more asymmetric drops corresponding to larger rain rates, the size and shape dependent backscatter intensities and depolarization pattern can in principle be attributed to rain rate [22]. According to the research report [33], Macke and Großklaus used the theory to visualize the geometries of the equilibrium raindrop shapes with scattering by radar and microwave wavelengths [22]. Though there is no radar and microwave implemented into the cases we study in this thesis, the geometries shown by Macke and Großklaus can give us some inspiration to understand why the Concave propeller perform worse and the Dome propeller surprisingly behave a little better.

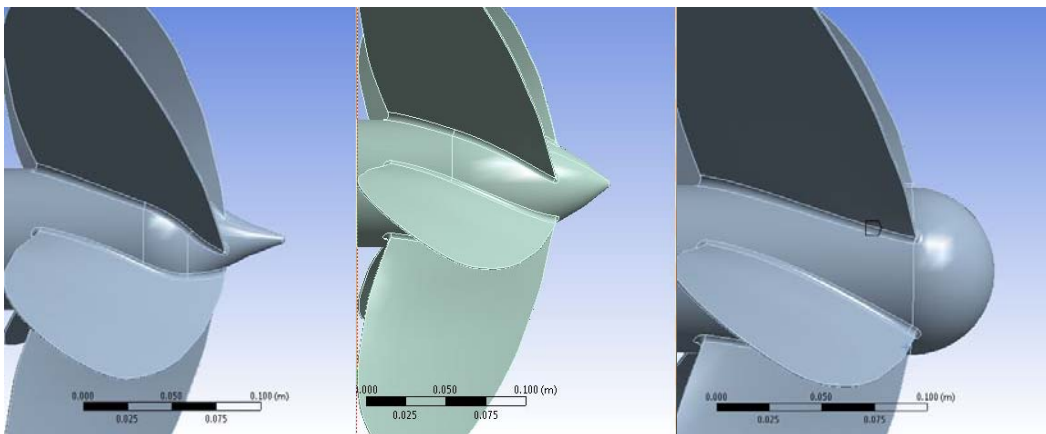


Figure 5-1 Hub part of the Concave propeller (left), the Convex propeller (middle), and the Dome propeller (right)

From the Figure 5-2 supported by [22], when the falling raindrop get the equilibrium with the radar or the microwave, when geometry is closed to the hub geometry of the Dome propeller. Calculations and details can be found in [22], but performances from Figure 4-10 can well state that when rotating speed is getting higher, the Dome propeller has a bigger mass flow compared to other propellers, especially at the RPM of 100rev/min.

The relative mass flows from Figure 4-10 at RPM of 70rev/min seems quite far from other points without an expectation. It can be inferred the mass flow of the Convex propeller here might not have a trustable result due to the mesh or the time step. So future work should be done with it later.

As for the high speed of the rotation applied into the Convex propeller, the Dome propeller, and the Center propeller, the mass flows at the outlet from these three propellers present the tendency respectively. The characteristics of the Center propeller surprise us with a better performance than the one within the condition of the low rotating speed from Figure 4-11. The mass flows captured at the RPM of 500rev/min, 750rev/min, 1000rev/min, and 1250rev/min are further elucidated in Figure 4-11. The Dome propeller possibly performs in a stable level

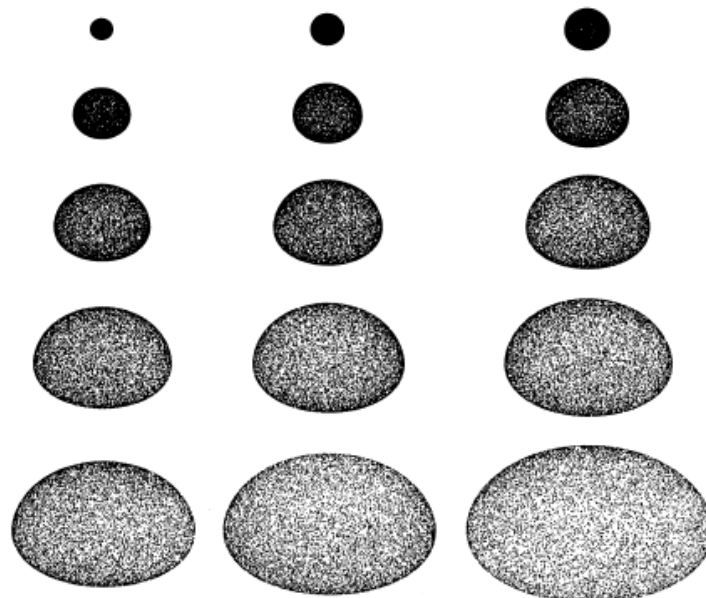


Figure 5-2 Geometry of equilibrium raindrop shapes.

Particle radii are (from left to right and from top to bottom) 0.5, 0.75, 1.0, 1.25, 1.5, 1.75, 2.0, 2.25, 2.5, 2.75, 3.0, 3.25, 3.5, 4.0, and 4.5mm [22]

among these propellers. However, the results from Figure 4-11 are done in a total time of 1 second and the time step of 0.05s. When the same total time applied into these models but a smaller time step of 0.03s, the results display an inconsistency with the predicted mass flow. But the mass flow is stable through the monitoring surfaces which can be checked in Table 5-1. There is no remarkable change between the four surfaces which means the fluid flow is stable. However, it should be noted that the mass flow at a higher speed should drag more fluid compared to the rotation velocity performed with RPM of 500rev/min, 750rev/min, 1000rev/min, and 1250rev/min. The reason of the unexpected results might be the time step. But a smaller time step with a higher speed followed the CFL criteria should present a better accuracy.

The dynamic performances of propellers are estimated by employing the standard $k-\epsilon$ turbulence model, suggesting the Dome propeller has a better performance dragging fluid flow compared with the Concave propeller, the Convex propeller, and the Center propeller.

The shear stress transport turbulence model is carried out to investigate the dynamic performance of propellers with a high rotating speed. As presented in Figure 4-11, the mass flows are recorded ranging from RPM of 500rev/min to RPM of 1250rev/min, suggesting the Center propeller behaved better than the Dome propeller, and the Convex propeller.

Because the instable fluid flow passing through the Winglet propeller, the calculated results of the mass flow cannot be trusted. It is reasonable that the time step processed during the simulations should be smaller. Therefore, this study of the winglet may offer a wrong

Table 5-1 Mass flow at RPM of 1500 rev/min with the time step of 0.03s

Type of Propeller	Mass flow at Inlet (kg/s)	Mass flow at Interface (kg/s)	Mass flow at Interface AB (kg/s)	Mass flow at Interface BC (kg/s)	Mass flow at Outlet (kg/s)
Convex propeller	1092.54	1092.64	1092.55		1092.46
Dome propeller	370.099	370.532	370.089		369.744
Center propeller	384.094	384.469	384.666		384.238

suggestion for the model. As for the Torqueedo propeller, it will be describe later in the future work part.

5.2 Discussion of Growing Velocity

The small time step is highly desirable in the process of the simulations. The smallest time step chosen in this thesis is 0.005s with a total time of 10 seconds applied into the Convex propeller. The monitored speed reports the tendency of the growing data, however, there is a decrease happened at the steps around 300 to 400 which is described in Figure 4-1.

It can be estimated that the turning point of the velocity occurs from 1.5s to 2s. Because there is no residence in our simulations models, the velocity is supposed to increase. Along the tails of the house of the Convex propeller, the vortices occur in the position like shown in Figure 5-3. According to the theory and research result from Prof. Kuhlmann [34], the energy transfer which can be visible near the vortex cores. This theory can be contributed to explain the decrease of the velocity coping with the Figure 5-4. The total time of the simulation in Figure 5-3 is 10 seconds. And the estimated turning point happens at the time of 1.5 and 2s.

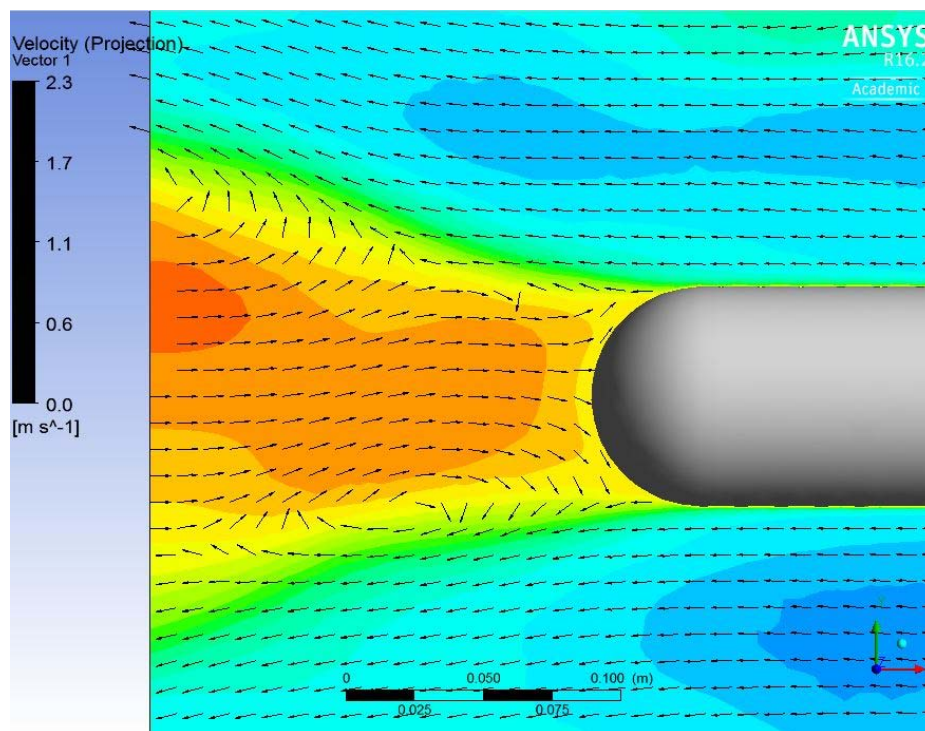


Figure 5-3 Velocity vectors of Convex propeller with total time of 10s and the time step of 0.005s

It can be checked that when the total time is 2 second, the vortices does not occur at the tail of the house of the Convex propeller, but happens closer to the blades, further than the tail of the house. The vortices here might rotates to cause a resistance for the fluid flow which is dragged by the propeller in a result with a decrease of the velocity of the flow. When the simulation time is 10 seconds, the vortices will move to the tail of the house, like presented in Figure 5-3, but because the total simulation time of 2 second is not that long enough for the vortices move to a further place, it might influence the velocity of the flow like the data monitored in the simulation which is shown in Figure 4-1. Due to the principle of the fluid mechanics, the fluid flow will be influenced by a nonlinear resistance which is perpendicular to the flow direction of the fluid flow. Therefore, regular vortices will be generated along two sides of the fluid. The frequency of the vortices is in a linear relation with the velocity of the flow [35].

$$f \approx \frac{S_v}{d} \tag{5-1}$$

Where:

v is the velocity of the flow

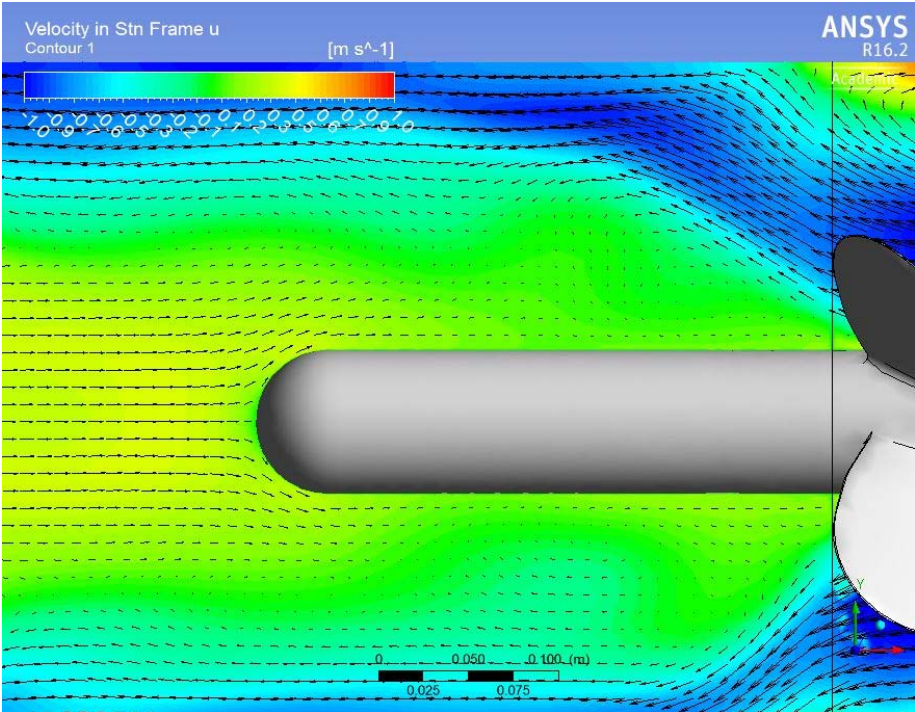


Figure 5-4 Velocity vectors of Convex propeller with total time of 2s and the time step of 0.005s

d is the horizontal dimension of the object in the flow

S is the Strouhal number, related with Reynolds number

It is clear to conclude that the frequency of the vortices has a linear relation with the velocity of the fluid flow. So when the propeller works for a while providing a high enough velocity, the vortices will appear.

From the simulations of different propellers, the mass flows are calculated due to the two turbulence flow models, the standard $k-\omega$ turbulence model and the shear stress transport turbulence model.

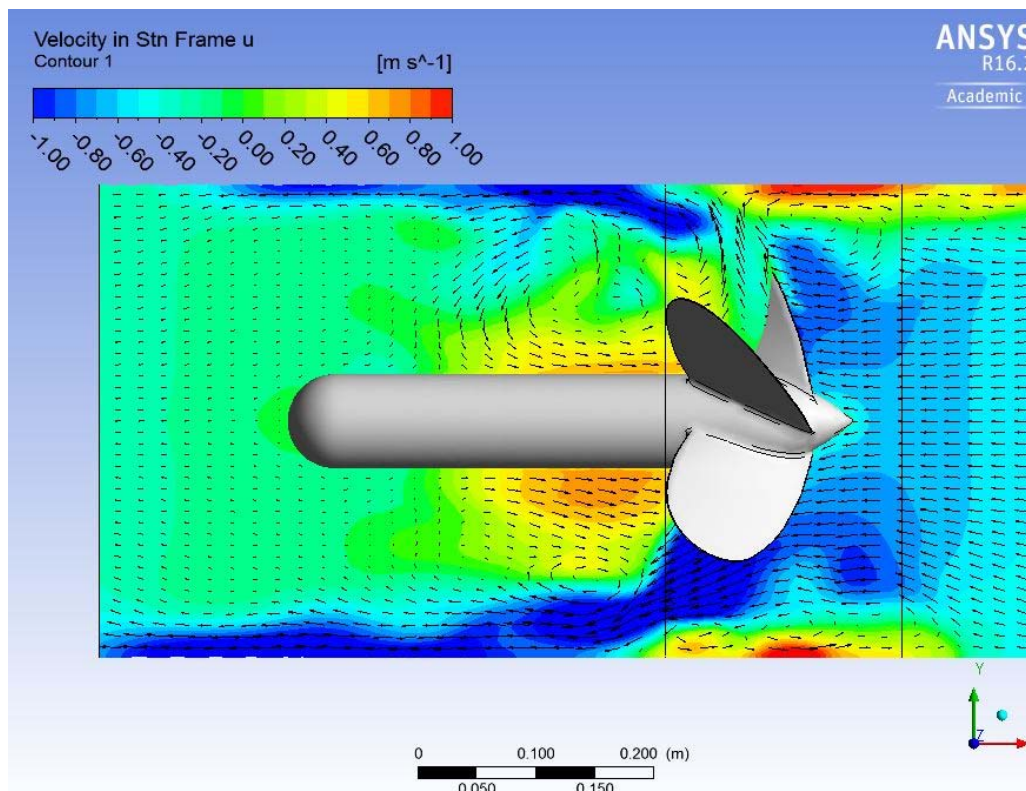


Figure 5-5 Velocity vectors of Convex propeller with total time of 1s and the time step of 0.005s

5.3 Recommendation for Future Work

There are many issues that can be addressed in future work. Here some of them are listed.

5.3.1 Time Step

5.3.1.1 Low Speed

In terms of the mass flow got from simulations shown in Figure 4-10, an unexpected mass flow at RPM of 70rev/min manifests the importance of choosing a proper time step. With the limitation of the computational time, in this thesis, a smaller time step will cause too much time to finish one simulation. Like the results shown in 4.2, the mass flow is in accordance with the time step and the total time. In addition, if we have enough time, the total time for the simulation should also be extended to figure out more information for the vortices and the stability.

5.3.1.2 High Speed

According to Figure 4-11, there are only four points in each curve, if we have time, it is better to test more points of the mass flow at different RPMs with the high speed. The impact of this work might change the tendency of the curves.

5.3.2 Reference Number for High Speed

For the high speed rotation, the reference number is got at the time step of 0.01s. However, it is possible to conclude the time step is not small enough due to the jump of the point of the mass flow within the total time of 1 s and the time step of 0.02s, with the RPM of 1500rev/min. When the rotation speed increases till 3000 rev/min, from Figure 4-5, we cannot obtain a smooth curve of the mass flow while the time step changes. It means the fluid flow with these time steps cannot reach the stability. It is a comparative result we got for the propellers at RPM of 1500rev/min, but with some errors. So the smaller time step is needed for RPM of 1500rev/min and RPM of 3000rev/min until we find the reference number for the mass flow within a stable flow. Then the results can be fully trusted.

5.3.3 Torqeedo propeller

The mesh of the Torqeedo propeller with eight blades is shown in Figure 3-13.

Applied with the same setting like described in Table 3-5, the shear stress transport turbulence model is applied into this model. However, the analysis process cannot be run in ANSYS. There are several reasons for that.

- Is the physics of the simulation set up correctly?

Yes, the physical model and simulation settings are all implemented into other propeller models.

- Is the mesh of high enough quality?

Maybe this is the reason, but according to the limitation of the nodes we can have via the student license, it is better not to change the mesh.

- Is a better initial condition required?

The initial condition is fine because at the beginning of the simulation, the propeller has no velocity, leading an initial velocity to be zero.

- Does this model require small time step to start?

As for this reason, it is necessary to try with different time step.

Chapter 6 Conclusion

In this report, we outline two methods, the standard $k - \varepsilon$ turbulence model and the shear stress transport turbulence model, for operating the analysis process for the low speed rotation and the high speed rotation applied into the propellers. The same settings for the mesh within the situation of low rotating velocities are implemented into the Convex propeller, the Concave propeller, the Dome propeller, and the Center propeller. We use the Convex propeller to be the reference model, compared with the other three propellers, due to the convenience and clearness of using the relative mass flow. From Figure 4-9, the mass flow changed by the rotating speed is highly described that propellers with high speed will create a stronger force to drag more fluid in the working domain. To determine the comparable dynamic performances of these four kinds of propellers, relative results are carried out to study the series of samples during the simulations with growing rotating speed. Figure 4-10 shows that the Concave propeller performs worst in the range of RPM of 10rev/min to PRM of 100rev/min.

When the RPM is varied from 10rev/min to 40rev/min, the Dome propeller and the Center propeller perform better than the Convex propeller. However, if the rotating speed grows, the Convex propeller has a better performance than the Dome propeller and the Center propeller. When the RPM is in the range of 90rev/min to 100rev/min, the Dome propeller has the largest mass flow among the four propellers. It means the Dome propeller has a better dynamic performance.

The Convex propeller, the Dome propeller, the Center propeller, and the Winglet propeller are compared with a high rotating velocity. When the RPM is changed from 500rev/min to 1250rev/min, the Center propeller has a better performance among the three propellers which is shown in Figure 4-11. However, when the RPM is 1500rev/min, the mass flow of the Dome propeller and the Center propeller is quite small, higher rotating velocities and smaller time step is required to be implemented in the future.

Bibliography

- [1] W. L. Oberkampf and T. G. Trucano, “Verification and validation in computational fluid dynamics,” *Prog. Aerosp. Sci.*, vol. 38, no. 3, pp. 209–272, Apr. 2002.
- [2] R. Patrick J., *Computational fluid dynamics*. Albuquerque: Hermosa Publishers, 1972.
- [3] K. J. Badcock, B. E. Richards, and M. A. Woodgate, “Elements of computational fluid dynamics on block structured grids using implicit solvers,” *Prog. Aerosp. Sci.*, vol. 36, no. 5, pp. 351–392, 2000.
- [4] G. Kuiper, “New developments and propeller design,” *J. Hydrodyn.*, vol. 22, no. 5 SUPPL. 1, pp. 7–16, 2010.
- [5] “Computational Fluid Dynamics.” [Online]. Available: https://www.wikiwand.com/en/Computational_fluid_dynamics. [Accessed: 18-Apr-2016].
- [6] L. Richard and S. Chapman, *Weather prediction by numerical process*. Dover Publications, 1965.
- [7] F. H. Harlow, “Fluid dynamics in group T-3 Los Alamos National Laboratory (LA-UR-03-3852),” *J. Comput. Phys.*, vol. 195, no. 2, pp. 414–433, 2004.
- [8] M. W. Evans, F. H. Harlow, and E. Bromberg, “The Particle-In-Cell Method for Hydrodynamic Calculations,” 1957.
- [9] T. C. Gillmer and B. Johnson, *Introduction to Naval Architecture*. Annapolis, Maryland: Naval Institute Press, 1982.
- [10] J. Carlton, *Marine Propellers and Propulsion*, Third. Butterworth-Heinemann, 2012.
- [11] S. Gaggero, C. M. Rizzo, G. Tani, and M. Viviani, “Design , analysis and experimental characterization of a propeller in decelerating duct,” no. May, pp. 227–235, 2013.
- [12] “Comparison Test: Boat Props,” 1997. [Online]. Available: <http://www.popularmechanics.com/adventure/outdoors/a5650/1276976/>. [Accessed: 01-May-2016].
- [13] E. Tupper, *Introduciton to Naval Architecture*, Third. Butterworth-Heinemann, 1996.
- [14] “Derivation of the Navier-Stokes equations.” [Online]. Available: https://www.wikiwand.com/en/Derivation_of_the_Navier%E2%80%93Stokes_equations. [Accessed: 10-May-2016].

- [15] W. H. Lam, D. J. Robinson, G. A. Hamill, and H. T. Johnston, “An effective method for comparing the turbulence intensity from LDA measurements and CFD predictions within a ship propeller jet,” *Ocean Eng.*, vol. 52, pp. 105–124, 2012.
- [16] D. Choudhury, “Introduction to the Renormalization Group Method and Turbulence Modelling,” *Fluent Inc. Tech. Memo.*, p. TM–107, 1993.
- [17] H. Versteeg and W. Malalasekera, *An introduction to computational fluid dynamics: the finite volume method*. Pearson Education, 2007.
- [18] W. Lam, G. A. Hamil, Y. C. Song, D. J. Robinson, and S. Raghunathan, “A review of the equations used to predict the velocity distribution within a ship’s propeller jet,” *Ocean Eng.*, vol. 38, no. 1, pp. 1–10, 2011.
- [19] D. Wilcox, *Turbulence Modelling for CFD*. La Canada, California: DCW Industries, 1998.
- [20] F. Menter, “Two-equation eddy-viscosity turbulence models for engineering applications,” *AIAA J.*, vol. 32, no. 8, pp. 1598–1605, 1994.
- [21] F. R. Menter, “Review of the shear-stress transport turbulence model experience from an industrial perspective,” *Int. J. Comput. Fluid Dyn.*, vol. 23, no. 4, pp. 305–316, 2009.
- [22] A. Macke and M. Großklaus, “Light scattering by nonspherical raindrops,” *J. Quant. Spectrosc. Radiat. Transf.*, vol. 60, no. 3, pp. 355–363, 1998.
- [23] “Propeller Technology.” [Online]. Available: <http://www.torqueedo.com/us/en-us/technology-and-environment/propeller-technology.html>. [Accessed: 11-May-2016].
- [24] “How these simple scimitar winglets make the 737 a whole new plane.” [Online]. Available: <http://gizmodo.com/how-these-simple-scimitar-winglets-make-the-737-a-whole-837341873>. [Accessed: 11-May-2015].
- [25] “Types of mesh.” [Online]. Available: https://www.wikiwand.com/en/Types_of_mesh. [Accessed: 12-May-2016].
- [26] S. Owen, S.J. Saigal, “Surface Mesh Sizing Control,” *Int. J. Numer. Methods Eng.*, vol. 47, no. January 1999, pp. 497–511, 2000.
- [27] T. D. Canonsburg, “ANSYS CFX-Solver Modeling Guide,” vol. 15317, no. November, pp. 724–746, 2013.
- [28] ANSYS Inc., “Mesh quality.” [Online]. Available: <http://www.afs.enea.it/project/neptunius/docs/fluent/html/ug/node167.htm>. [Accessed: 13-May-2016].

- [29] F. Trivellato and M. Raciti Castelli, “On the Courant-Friedrichs-Lewy criterion of rotating grids in 2D vertical-axis wind turbine analysis,” *Renew. Energy*, vol. 62, pp. 53–62, 2014.
- [30] H. H. S. Price, R. S. R. R. S. R. Varga, and J. E. Warren, “Application of oscillation matrices to diffusion-convection equations,” *J. Math. Phys.*, vol. 45, no. 3, pp. 301–311, 1966.
- [31] A. Daus, E. Frind, and E. Sudicky, “Comparative error analysis in finite element formulations of the advection-dispersion equation,” *Adv. Water Resour.*, vol. 8, no. 2, pp. 86–95, 1985.
- [32] K. P. Company, “Kamome Propeller.” [Online]. Available: <http://www.kamome-propeller.co.jp/en/products/propeller/fpp/>. [Accessed: 21-Apr-2016].
- [33] C. Chuang and K. V. Beard, “A numerical model for the equilibrium shape of electrified raindrops,” *J. Atmos. Sci.*, vol. 47, no. 1, pp. 1374–1389, 1990.
- [34] S. Albensoeder and H. C. Kuhlmann, “Three-dimensional instability of two counter-rotating vortices in a rectangular cavity driven by parallel wall motion,” *Eur. J. Mech. B/Fluids*, vol. 21, no. 3, pp. 307–316, 2002.
- [35] B. Green, *Fluid Vortices*, Illustrate. Springer Science & Business Media, 2012.
- [36] “Boeing 737-700.” [Online]. Available: http://www.aviationpartnersboeing.com/products_737_700.php. [Accessed: 11-May-2016].